This is to certify that the
thesis entitled

CHARACTERIZATION OF THE SEQUENCE AND SUBSTRATE REACTIVITY OF DIHYRDONEOPTERIN ALDOLASE AND ITS SITE-DIRECTED MUTANTS BY TANDEM MASS SPECTROMETRY

presented by

Gwynyth Scherperel

has been accepted towards fulfillment
of the requirements for the

M.S. degree in Chemistry

Major Professor's Signature

11/27/2006

Date

CHARACTERIZATION OF THE SEQUENCE AND SUBSTRATE REACTIVITY OF DIHYDRONEOPTERIN ALDOLASE AND ITS SITE-DIRECTED MUTANTS BY TANDEM MASS SPECTROMETRY

BY

GWYNYTH SCHERPEREL

A THESIS

Submitted to
Michigan State University
In partial fulfillment of the requirements
For the degree of

MASTER OF SCIENCE

Department of Chemistry

2006

ABSTRACT

CHARACTERIZATION OF THE SEQUENCE AND SUBSTRATE REACTIVITY OF DIHYDRONEOPTERIN ALDOLASE AND ITS SITE-DIRECTED MUTANTS BY TANDEM MASS SPECTROMETRY

BY

GWYNYTH SCHERPEREL

The gas-phase fragmentation reactions of a series of site-directed mutagenesis products of *Staphylococcus aureus* dihydroneopterin aldolase (SaDHNA) were examined in order to explore the utility of the linear quadrupole ion trap (LIT) for 'top down' proteomics. It was found that multistage tandem mass spectrometry (MS/MS and MS^3) coupled with high resolution resonance ejection scans in the ion trap may be employed for the routine 'top down' characterization of recombinant proteins of modest (<20 kDa) size. The effect of single amino acid mutations on the charge state dependent gas-phase fragmentation behavior of intact protein ions was also explored. Four mutants gave fragmentation similar to that of the wild-type (WT) protein, but two resulted in substantially different product ion spectra. This restricted the ability to localize the modification site of these mutants and illustrated the effect that single amino acid mutations can have on fragmentation behavior. The reactions of the WT SaDHNA protein and its Y61F mutant with the substrate 7,8-dihydroneopterin (DHNP) were also examined by tandem mass spectrometry in order to determine the structure-function role of the tyrosine residue. The WT reaction formed the expected product 6-hydroxymethyl-7,8-dihydroneopterin (HP). The Y61F reaction, however, yielded a different product, subsequently found to be 7,8-dihydroxanthopterin (DHXP). This led to the proposal that the Y61F mutant changes the function of the enzyme from an aldolase to an oxygenase.

ACKNOWLEDGMENTS

This project would not have been possible without the support of many people. First, I would like to thank my research advisor, Dr. Gavin E. Reid, for his guidance, encouragement, and support during my graduate study. I would also like to thank my committee members, Dr. David Weliky and Dr. Gary Blanchard, for their guidance and support. Ms. Katherine Rank was vital to the completion of this project and deserves many thanks for the data analysis she did for some of the SaDHNA charge states. This project could not have been completed without the help of Dr. Yi Wang who performed some preliminary experiments regarding the substrate reactivity research. Many thanks also to Dr. Honggao Yan who, along with Dr. Wang, provided a seemingly unending supply of proteins. I would also like to acknowledge Dr. Kade Roberts who performed the initial mass spectrometry experiments in regards to the substrate reactivity research. He was a crucial player in the determination of the mechanisms used by the different mutants, as well as the products they produce. Dr. Roberts taught me many things when I was still a novice at mass spectrometry and he, along with Ms. Rank and Dr. Wang, have become good friends. I would also like to thank previous and current group members of the Reid research group for the friendship, help, and motivation. In particular, special thanks goes to Mahasilu Amunugama, Jennifer Froelich, and James Sierakowski who helped me become a better scientist, answered my numerous questions, and became good friends along the way. Finally, I would like to thank my parents and friends who endured this long process with me, always offering support and encouragement.

TABLE OF CONTENTS

LIST OF FIGURES

LIST OF TABLES

LIST OF SCHEMES

CHAPTER ONE

INTRODUCTION

1.1 Proteomics

Proteomics has recently emerged as an important research field due to the success of worldwide genome sequencing efforts. Proteomics involves the comprehensive identification, characterization, and quantitative analysis of the gene products, i.e., proteins, and their specific functional interactions, expressed by a particular cell or tissue type at a given time throughout the cell cycle, or under a particular type of stimulation, e.g., healthy versus diseased states. However, in contrast to the static genome, the proteome is a dynamic entity, as proteins are continuously being synthesized, modified, or degraded, not only to carry out the desired functions of a cell, but also in response to disease or injury [1]. These changes in protein expression or modification state may potentially be used to identify specific biomarkers for the early diagnosis of disease [2].

---

* The concepts discussed in this Chapter will be published in: Scherperel, G.; Reid, G. E. Emerging methods in proteomics research: multistage tandem mass spectrometry for top-down protein characterization. *The Analyst* **2006** *(Invited review article to Education i-section).*

1.2 Mass Spectrometry

Mass spectrometry, which measures the mass-to-charge ratio (m/z) of an ion, has become the key enabling technology for proteomics. In particular, the speed, sensitivity, and specificity of mass spectrometry make it the preferred approach for rapid protein identification and characterization studies. A mass spectrometer consists of the components illustrated in Figure 1.1.

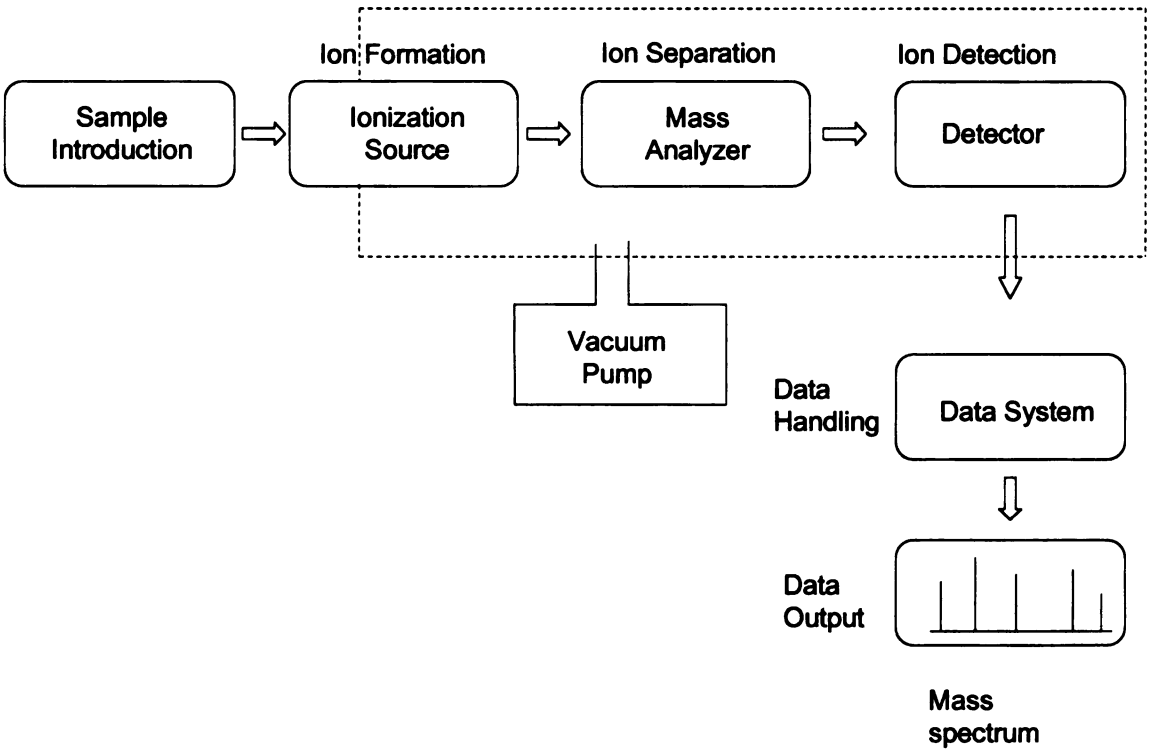

Figure 1.1 Components of a mass spectrometer (adapted from "What is Mass Spectrometry". www.asms.org).

1.2.1 Methods for the Ionization of Biological Molecules

The first component of a mass spectrometer is the ionization source, which is responsible for the conversion of molecules to ions. During the mid 1980's, two ionization techniques were developed, namely matrix assisted laser desorption ionization

(MALDI) [3] and electrospray ionization (ESI) [4], that enabled the facile 'soft' ionization and transfer of large non-volatile thermally labile biological molecules into the gas-phase. MALDI, developed by Karas and Hillenkamp [3], utilizes the impact of high energy photons from a laser on a sample imbedded in a solid organic crystalline matrix to ionize analytes and to produce predominantly singly charged pseudomolecular (e.g., $[M+H]^+$) ions. Samples are dissolved in a matrix containing a UV absorbing chromophore and co-crystallized onto a metal target. This target is then placed under vacuum in the ion source and bombarded with short duration laser pulses. This causes the sample to heat up and the sample and matrix to sublime; the matrix absorbs most of the energy from the laser making this is a soft-ionization technique.

ESI, developed by Fenn *et. al.* [4], involves dissolving the sample in a liquid solvent and then pumping this through a small diameter capillary tubing. The capillary tip, located at atmospheric pressure, is floated at high potential causing the formation of an electric field which induces charge accumulation at the surface of the liquid. When a high enough voltage is applied to break the surface tension of the solvent, a Taylor cone forms and an electrospray of charged droplets begins. Gaseous ions are then produced as these charged droplets undergo solvent evaporation, due to high temperature or the presence of a sheath gas, and coulomb fissions, due to either the charge residue model (CRM) [5] or the ion evaporation model (IEM) [6, 7]. The CRM argues that a sequence of Rayleigh instabilities (where columbic repulsion becomes greater than the surface tension) and periods of solvent evaporation produce final droplets that contain only one ion each. This ion is then liberated into a gas-phase ion as the last of the solvent evaporates. The IEM, on the other hand, proposes that before a droplet reaches the final

stage in the CRM model, where it contains only one ion, the field on the droplet's surface becomes strong enough to overcome the solvation forces, allowing an ion to escape from the droplet surface and enter the gas phase. It is thought that large molecules ionize according to the CRM, while the dominant mechanism for smaller molecules may be the IEM.

ESI can be used in a direct infusion mode or coupled with high performance liquid chromatography (HPLC). In the direct infusion mode, analytes are dissolved in an appropriate solvent, such as methanol/water (1:1), and introduced into the mass spectrometer at the desired flow rate via a syringe pump. When coupled with HPLC, the analytes are dissolved in the appropriate HPLC solvent and are subjected to ESI directly as they elute off the column.

One of the most important features of ESI is the formation of a series of both singly and multiply charged pseudomolecular ions (typically formed by protonation). This multiple charging effect enables the m/z ratios of high molecular weight proteins to be observed within the range of a variety of mass spectrometers and allows for the analysis of a variety of m/z states for a given analyte, thus improving mass accuracy and potentially improving sequence coverage by providing access to different fragmentation reaction channels in tandem mass spectrometric experiments. Multiply charged precursor ions also enable greater energy deposition for the dissociation of large protein ions because the power absorbed by an ion during excitation increases with the square of its charge [8]. The extent of multiple charging is influenced by the composition and pH of the electrospray solvent, as well as the chemical nature of the analyte.

1.2.2 Mass Analyzers and Detectors

The purpose of the mass analyzer component of the mass spectrometer is to separate mixtures of gas-phase ions according to their m/z ratios. A range of mass analyzers exists for this purpose, each with their own unique capabilities and operational performance characteristics (e.g., resolution, sensitivity, mass accuracy). Four types of mass analyzers are typically used for proteomics: (i) quadrupole, (ii) quadrupole ion trap, (iii) time of flight (TOF), and (iv) Fourier transform ion cyclotron resonance (FT- ICR) analyzers. The quadrupole ion trap and FT-ICR mass analyzers are discussed in the following sections. The remaining components of the mass spectrometer are the detector that converts the ion flux into a proportional electric current and a data system that records the magnitude of this electrical signal as a function of mass-to-charge (i.e. a mass spectrum).

1.2.2.1 The Quadrupole Ion Trap Mass Analyzer

The quadrupole ion trap is an electrodynamic mass analyzer consisting of a ring electrode and two end caps. A variable amplitude radio frequency (RF) is applied to the ring electrode to create a three dimensional quadrupole electric field to trap ions within the region bound by the electrodes. By adding a small amount of bath gas, such as helium, the motion of ions injected into the trap can be dampened, thereby increasing their trapping efficiency. The potential applied to the ring electrode can be given by the equation

$$\Phi_0 = + (U\text{-}V\cos \omega t) \quad (1)$$

where U is the amplitude of the direct current (DC) potential, V is the amplitude of the applied alternating current (AC) potential (in the RF range), ω is the angular frequency (ω = 2πυ, where υ is the frequency of the applied RF), and t is time. The field is seen in three dimensions, thus the motion of the ions under the influence of the applied potentials occurs in three dimensions: x, y, and z. Due to the cylindrical symmetry of the trap x equals y and the ion motion can be expressed using the coordinates z and r. Thus, the equations of motion inside the trap can be shown to be

$$\frac{d^2z}{dt^2} - \frac{4e}{m\left(r_0^2 + 2z_0^2\right)}(U - V\cos\omega t)z = 0 \tag{2}$$

$$\frac{d^2r}{dt^2} + \frac{2e}{m\left(r_0^2 + 2z_0^2\right)}(U - V\cos\omega t)r = 0 \tag{3}$$

where r and z are the distances from the center of the trap to the ring and exit electrodes, respectively, and **z** is the charge on the ion.

Similarities can be seen when comparing these two equations with the Mathieu equation given below.

$$\frac{d^2u}{d\xi^2} + (a_u - 2q_u\cos 2\xi)u = 0 \tag{4}$$

In this equation, u can stand for either z or r in equations (2) and (3) and $\xi = \frac{\omega t}{2}$. Thus, the equations of ion motion given can be written in the form of the Mathieu equation:

$$a_u = a_z = -2a_r = \frac{-16ze\Theta U}{m(r_0^2 + 2z_0^2)\omega^2} \tag{5}$$

$$q_u = q_z = -2q_r = \frac{4zeV}{mr_0^2\omega^2} \tag{6}$$

$$q_z = \frac{8zeV}{m(r_0^2 + 2z_0^2)\omega^2} \tag{7}$$

where U is the DC potential, V is the amplitude of the RF potential, m is the mass of an ion, r_o is the distance from the center of the trap to the ring electrode, z_o is the distance from the center of the trap to the exit electrodes, and ω is the angular velocity of the RF potential; r_o, z_o, and ω are constant for a given trap. There is no applied DC potential in three dimensional ion trap mass analyzers, thus the a_u term from the Mathieu equation equals zero. The solution for the dimensionless trapping parameter q_u (related to the RF potential, V) is therefore the critical parameter. Equation (6) is the solution for an ideal ion trap, while equation (7) is for a 'stretched' quadrupole ion trap. A 'stretched' trap is one where the distance between the end caps has been increased to introduce a negative higher order field (i.e. octapole) component to offset the positive higher order field introduced by truncation of the potential field from the ion trap electrodes.

Ions are stable in the ion trap as long as their trajectories do not reach the distances r_0 and z_0. By plotting a_u versus q_u, the areas where ions of a given mass-to-charge ratio (m/z) are stable, i.e. do not reach values above or equal to r_0 or z_0, as a function of the applied RF frequency and amplitude, can be determined. Figure 1.2 shows such a stability diagram for a 3D quadrupole ion trap [9]. As there is no applied DC potential, all of the ions line up along the x-axis of the stability diagram. According to equations (6) and (7), q is directly proportional to V, but inversely proportional to m/z. Thus, for a given m/z, as V is increased ions move along the x-axis towards higher q values. Ions will become unstable as they reach the boundary of the stability region, at a q value of 0.908, and be ejected from the trap. Thus, a mass spectrum may be acquired by scanning the amplitude of the RF field (V) applied to the ring electrode to progressively destabilize ions of increasing m/z value. This, however, is not the most efficient manner to eject ions from a trap because several m/z ions can be ejected at essentially the same time due to the slope of the potential well in which ions are trapped (discussed later), thereby resulting in loss of resolution.

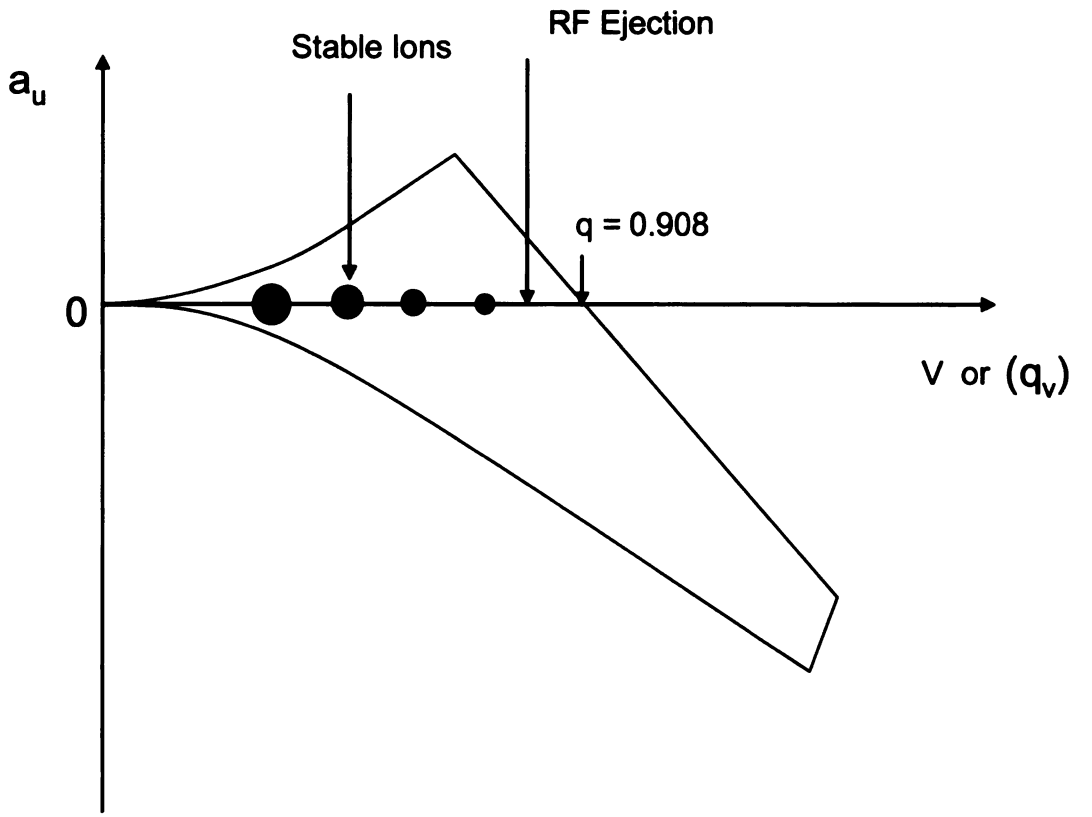

Figure 1.2 Typical Mathieu stability diagram for quadrupole ion trap. The larger balls represent high mass ions whereas the smaller balls represent low mass ions. (Reproduced and modified from reference 8)

One solution to overcome this is to use resonance ejection. It was noted earlier that υ is the frequency of the applied RF field. Ions in the trap, however, do not oscillate at this fundamental frequency because of their inertia. They will oscillate at a secular frequency f that is lower than υ. The relationship between f and υ along the z axis is given by

$$f_z = \frac{\beta_z v}{2} \tag{8}$$

where β_z is a fundamental stability parameter given by the approximation

$$\beta_u = \left[a_u + \left(\frac{q_u^2}{2} \right) \right]^{1/2} \tag{9}$$

for q_u values lower than 0.4. Since β_z equals one at the q value of 0.908 (where ions become unstable), the maximum secular frequency an ion can have is half the applied RF frequency. If a supplementary auxiliary AC (RF) signal, or 'tickle', is applied to the endcap electrodes, typically at a q value of 0.86, an ion's secular frequency can be slowly raised (by increasing V) until it matches the applied frequency on the endcaps, i.e., it is in resonance with the AC signal, and is ejected. The resolution obtained in the mass spectrometer is inversely proportional to the resonance ejection scan rate. Therefore, the slower V is increased, i.e. the slower the resonance ejection scan rate, the better the resolution.

Conventional 3D quadrupole ion trap instruments are prone to overfilling (space charge effects due to ion-ion coulombic repulsion), whereby the charge density increases beyond that where response is linear with respect to ion number, resulting in a decrease in mass analyzer resolution, and imposing a practical upper limit to ion accumulation levels, and ultimately, sensitivity. This problem has been largely overcome by the development of linear two dimensional (2D) quadrupole ion traps [10, 11], whereby ions are trapped in the x- and y-dimension by the application of an electrodynamic RF potential field to opposing pairs of quadrupole rods, and in the z-dimension by static DC potentials applied to electrodes situated at either end of the quadrupole. Linear 2D quadrupole ion traps

exhibit higher acceptance (i.e., more efficient ion injection) compared to 3D traps, due to the lack of a quadrupolar field along the z-axis, as well as orders of magnitude greater ion storage capacity, due to the larger volume of the device and the fact that ions are focused along the entire length of the quadrupole due to the radial nature of the quadrupolar confinement field.

The multistage tandem mass spectrometry (MS/MS and MS^n) capabilities of the ion trap make it particularly attractive as a mass analyzer for peptide and protein characterization studies. Tandem mass spectrometry involves the repeated isolation and fragmentation of ions, which occurs n times for an MS^n analysis. For example, an MS/MS experiment would involve a series of events consisting of isolation of a precursor ion, an intermediate reaction event (typically involving energetic dissociation), followed by mass analysis of the product ions [9]. Isolation of the selected precursor ion is performed by the application of a high amplitude 'notched' broadband resonance ejection supplementary RF signal applied to the end caps in order to eject all ions except the precursor ion of interest. The isolated ion is then subjected to fragmentation by collision induced dissociation (CID), through the application of a low amplitude RF resonance excitation signal applied to the end cap electrodes at a frequency corresponding to the secular frequency of motion of the ion of interest, to enable energetic collisions with the background He gas that is present. This causes some kinetic energy to be converted into internal energy, bringing the ion to a vibrationally excited state and resulting in fragmentation. The secular frequency of motion of the product ions are not in resonance with the supplemental RF signal and are therefore 'cooled' by collisions with the background gas to the center of the trap. More energy is required to fragment larger

molecules due to their greater number of vibrational modes. Thus, ion ejection may potentially occur prior to fragmentation. The Dehmelt pseudopotential well associated with ion storage in the ion trap is given by the equation

$$\overline{D_z} = q_z \frac{V}{8} = \frac{zeV^2}{m(r_0^2 + 2z_0^2)\omega^2} \tag{10}$$

where $\overline{D_z}$ is the Dehmelt potential. It is also illustrated in Figure 1.3, where the energy E_{RE} represents the energy that is required at a specified q value in order for an ion to be ejected due to resonant excitation. Dissociation is typically performed at a q value of 0.25 to maintain a balance between the requirement for obtaining efficient ion fragmentation (rather than ejection), while keeping an appropriate low mass cutoff value for storage of the resultant product ions. Note that increased columbic repulsion associated with multiply charged precursor ions acts to lower the energy required for the fragmentation of large proteins in the ion trap.

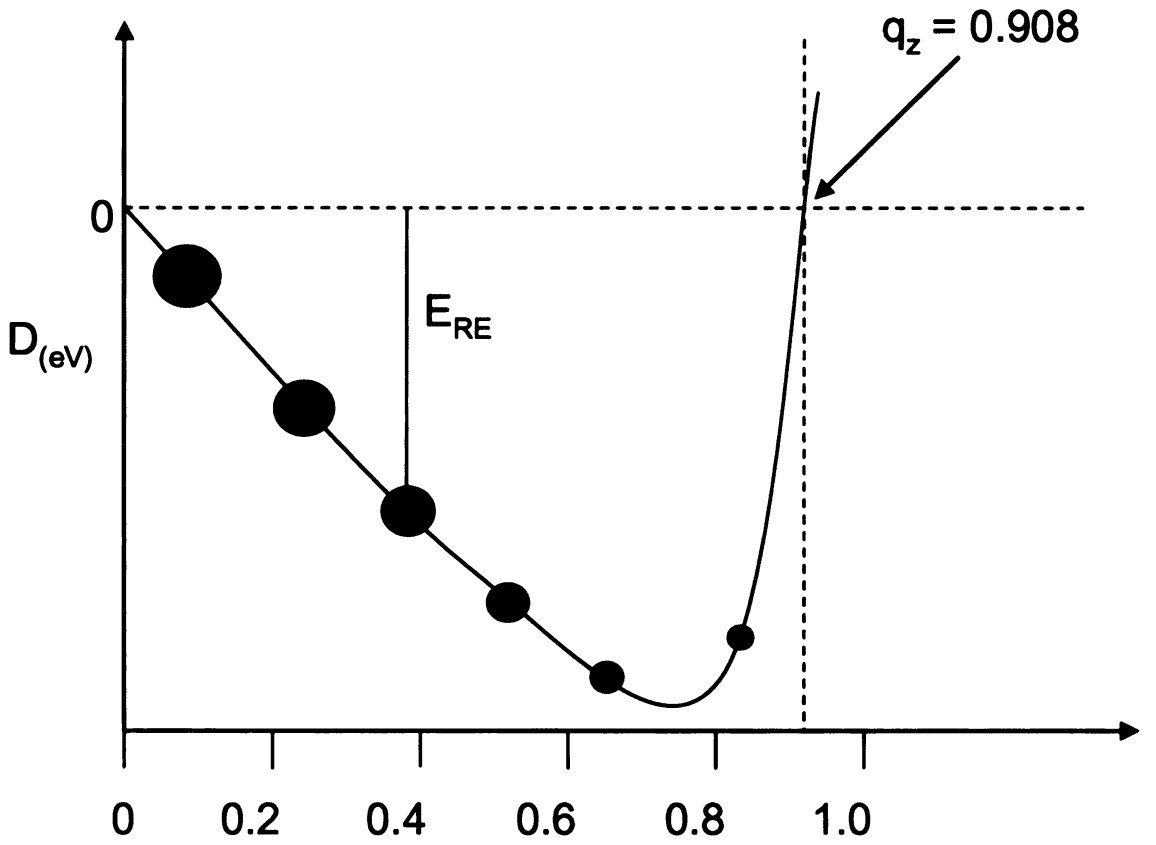

Figure 1.3 Dehmelt pseudo well potential D (eV) as a function q_z. Higher mass ions for a given V value have lower Dehmelt trapping energies. (Reproduced and modified from reference 8).

1.2.2.2 Fourier Transform Ion Cyclotron Resonance Mass Analyzer

Fourier transform ion cyclotron resonance (FT-ICR) mass analyzers trap ions in a three dimensional cell located within a strong magnetic field produced by a superconducting magnet. The three dimensional cell usually consists of three pairs of parallel plates, arranged as a cube, for ion trapping, excitation, and detection. Ions entering the homogenous magnetic field on a trajectory perpendicular to the magnetic field strength B will experience a centripetal force

$$F = zevB \tag{11}$$

where v is the velocity of the ion. This force is balanced by the centrifugal force

$$F' = \frac{mv^2}{r} \tag{12}$$

where r is the radius of the ion's arced trajectory. Combining equations (11) and (12) gives

$$zevB = \frac{mv^2}{r} \tag{13}$$

which rearranges to

$$r = \frac{mv}{zeB} \tag{14}$$

It can be seen from equation (14) that if the magnetic field (B) is large enough, the radius (r) will be small enough such that ions will be trapped in a circular trajectory in the x- and y-dimensions; a small DC potential is applied to the trapping plates of the cell to trap ions in the z-, or axial, dimension. When an ion becomes trapped in the x and y dimensions, it will complete one full cycle with a frequency, υ, of

$$\nu = \frac{v}{2\pi r} \tag{15}$$

This rearranges to give the cyclotron frequency, ω_c, of an ion in the x and y trapping dimensions

$$\omega_c = 2\pi\nu = \frac{v}{r} = \frac{zeB}{m} \tag{16}$$

where υ is the frequency of the circular trajectory, v is the velocity, r is the radius of the ion's circular trajectory, and B is the magnetic field strength.

Ions of each m/z have their own characteristic cyclotron frequencies. If a short RF excitation pulse is applied at the cyclotron frequency corresponding to a particular m/z, the 'resonant' ions will absorb energy and be brought into phase with the excitation pulse. When several different m/z are present a rapid frequency sweep ('chirp') or a tailored waveform excitation pulse that contains components at all the cyclotron frequencies can be applied. Ions excited by AC irradiation at their own frequency and with the same energy (thus the same potential V) applied over the same time, T, will have an orbit with the same radius, r, and thus all the ions will pass close to the detector plate.

$$r = \frac{VT}{B} \tag{17}$$

As seen in this equation, the radius of the ions is independent of the m/z ratio. Thus, broadband excitation will bring all ions onto the same radius, but at frequencies that are dependent on their m/z, provided that the voltage is the same at each frequency.

When the ions are excited they increase the radius of their orbit and pass closer to the detector plates. When a packet of positive ions approaches the first detector plate, electrons are attracted from ground through the external circuit and accumulate in the detector plate, causing a temporary current. As the ions continue to rotate and approach the second detector plate, the electrons move and accumulate there. This induces an alternating 'image' current whose amplitude is proportional to the number of ions and whose frequency is the same as the cyclotron frequency of the ions.

The image current contains frequency components from all of the m/z ratios present. The image current can be mathematically converted from a time domain signal to a frequency-domain signal (the mass spectrum) through the application of a Fourier transform, which separates a waveform into sinusoids of different frequencies that sum to the original waveform. Cyclotron frequencies can be measured with very high precision, allowing high accuracy mass measurement (< 1 ppm) and high resolving power (unit mass resolution of > 10^5) to be obtained. Residual neutrals and molecules present in the ICR cell dampen the coherent motion of the ions. Thus, in order to obtain ultra-high resolution, the ICR cell must be maintained at high vacuum.

The small DC potential applied to the trapping plates of the cell to keep the ions contained within it results in ion oscillation in the z, or axial trapping, dimension. Due to the three dimensional nature of the trapping cell, this axial ion motion results in an outward-directed electric force in the x and y trapping dimensions that opposes the inward-directed force from the applied magnetic field. This results in magnetron motion with a frequency, ω_m, of

$$\omega_m = \frac{\omega_z^2}{2\omega_c} \tag{18}$$

where ω_z is the frequency in the z dimension and ω_c is the cyclotron frequency. In the presence of collisions with the neutral bath gas, the ion magnetron radius (the radial position of the center of an ion cyclotron orbit) increases slowly over time, whereas the cyclotron radius decreases rapidly. By applying a two-dimensional azimuthal quadrupolar excitation at a frequency corresponding to the cyclotron frequency, however, the magnetron radius may be converted to a cyclotron radius. Collisions then rapidly dampen the cyclotron motion to zero and ions relax back to the center of the trap, giving a dynamic rise in resolution, sensitivity, and selectivity.

1.3 Current Approaches Employed in Proteomics

The two main mass spectrometry based approaches for proteomic studies today have been classified as 'bottom up' and 'top down'. Each of these is defined in more detail below. Both of these techniques commonly use tandem, or multi-stage, mass spectrometry to obtain more detailed structural information following the acquisition of intact precursor ion masses.

1.3.1 Bottom Up Proteomics

A 'bottom up' analysis is performed by initial proteolytic digestion of the protein of interest, usually with trypsin. Protein identification may then be achieved by 'peptide mass fingerprint' analysis, the comparison of the experimentally determined intact

peptide masses with the peptide masses obtained by theoretical digestion of the proteins contained within a sequence database [12]. Experimentally determined peptide masses that differ from predicted values are indicative of a modified region within the protein sequence, thereby allowing their rapid localization for subsequent fragmentation by MS/MS in order to identify and characterize the precise site of the modification. Following acquisition of an MS/MS product ion spectrum on a selected peptide precursor ion of interest, protein identification may be achieved by *de novo* sequence analysis [13] or by automated database search algorithms, such as Sequest [14] and Mascot [15]. These algorithms calculate a score or probability that describes how well an experimental product ion tandem mass spectrum agrees with a theoretical product ion spectrum generated by the search engine. The fragmentation behavior of peptide ions is generally well understood and the identification of peptides is relatively straightforward using MS/MS and database searching methods.

Unfortunately, 'bottom up' protein digestion strategies result in a large increase in the number of components to be analyzed. Thus, abundant peptides tend to be preferentially selected for MS/MS analyses over low abundance peptides. Furthermore, it is common that some of the peptides resulting from proteolytic digestion are not observed upon mass spectrometric analysis, thereby precluding their characterization. Also, it is relatively common that only partial sequence information can be derived from the dissociation of a protonated peptide ion. Finally, the mass of the intact protein, which may be informative regarding the modification state of the protein [16], is not obtainable by bottom up methods. Thus, complete characterization of a protein can be difficult to achieve using bottom up methods.

1.3.2 Top Down Proteomics

An initial step taken for the mass spectrometry based characterization of a recombinant protein involves the determination of its intact mass [16, 17]. This can be achieved by using high resolution (10^4–10^5) and mass accuracy (1–10 ppm) Fourier transform ion cyclotron resonance (FT-ICR) [18-22] and, albeit to a lesser extent, by using quadrupole ion trap mass spectrometry instrumentation [17]. Intact mass measurements provide a rapid initial assessment of protein purity, as well as providing evidence that the protein of interest has been correctly expressed and folded i.e., validation of the primary amino acid sequence and disulfide bond arrangement. The presence of many common expected and unexpected co- or post-translational modifications introduced to the protein by, for example, PCR errors, sequence variants, alternative splicing, N- and C-terminal processing, phosphorylation, glycosylation, oxidation etc., may often be deduced from these measurements, based on the mass differences observed between the experimental and predicted values [16, 17, 23]. Unfortunately however, the mass of the intact protein alone is generally not useful for characterization of these proteins, due to the inability to unambiguously localize co- or post-translational modifications to a specific site within the protein sequence.

There has been an increasing recognition in recent years therefore, of the potential for 'top down' tandem mass spectrometry based approaches to protein characterization. The product ion masses obtained by dissociation of intact protein ions may be compared to those predicted from the theoretical protein sequence, potentially allowing protein identification and characterization to be achieved in a single step [24, 25, 26], including any co- or post-translational modifications such as phosphorylation or glycosylation [23,

27]. Perhaps the most significant advantage of top down methods is that the initial mixture complexity is minimized by avoiding the protein digestion and sample processing steps that are characteristic of the bottom up approach.

Top down proteomic methods are not without their own challenges. The three main issues today involve (1) determination of the charge states and masses of the multiply charged product ions resulting from the dissociation of large multiply charged protein ions, (2) maximizing the extent of sequence coverage that may be obtained from these dissociation reactions, and (3) the availability of bioinformatic tools for high throughput data analysis. A number of current and potential future strategies to address these issues are discussed in more detail in the following sections.

1.4 Product Ion Charge State Determination

A key step in enabling top down approaches has been the ability to assign product ion identities resulting from the dissociation of multiply charged precursor ions. Product ion charge states can range from +1 up to the precursor ion's charge state. While it is simple enough to determine the m/z of a product ion, if the charge (z) can not be determined, the mass can not be determined, and subsequently the ion can not be identified. The charge state of an ion may be determined as the reciprocal of the difference in m/z between two adjacent isotopic peaks for a given ion. As the charge, or mass, of an ion increases, however, so does the resolution needed to distinguish the isotopic distribution and thus calculate charge. Solutions to this problem have come from (1) the development of instrumentation with high resolving power such that the individual isotopes of a multiply charged product ion can be resolved for charge state

determination and (2) the use of gas-phase ion/ion proton transfer reactions to reduce the charge states of multiply charged product ions to their singly charged forms, thereby readily enabling determination of their masses. As discussed later, ion/ion proton transfer reactions can also be used to manipulate precursor ion charge states and thus minimize mixture complexity prior to performing MS/MS.

1.4.1 High Resolution Instrumentation

In the past, the issue of charge state, and thus mass, determination was largely overcome by the use of high resolution (10^4–10^5) and high mass accuracy (1-10 ppm) Fourier transform ion cyclotron resonance (FT-ICR) mass spectrometry [18-22]. Resolution increases linearly with increasing magnetic field strength. Thus, one way to improve resolution, and mass accuracy, has been to increase the strength of the magnet. Magnets up to 15 T have recently become commercially available, while FT-ICR instrumentation containing magnets with field strengths up to 25 T have been developed at the National High Magnetic Field Laboratory in Florida [28].

More recently, Makarov *et. al.* have developed a new electrostatic mass analyzer (the Orbitrap) from which high mass accuracy (up to parts per million) and high mass resolution (up to 150,000) can be obtained [29, 30]. In the Orbitrap, ions are trapped about a central electrode where they undergo harmonic oscillations in the radial and axial dimensions. Since the frequency of ion oscillations in this dimension is independent of the energy and spatial spread of the ions, m/z values can be determined with high mass accuracy and resolution in the axial dimension. Just as with the FT-ICR mass analyzers,

the time-domain image current is converted to a mass spectra via the application of a fast Fourier transform (FFT).

Mass spectrometers such as the quadrupole ion trap are also beginning to find increasing use in high resolution top down protein identification/characterization studies [17]. As discussed in Section 1.2.2.1, resolution in ion trap instruments is inversely proportional to the resonance ejection scan rate. Thus, while quadrupole ion trap mass spectrometers are generally operated under low resolution conditions (>500, with mass accuracy ~ 300 ppm), high resolution performance (>17,000, with mass accuracy ~ 20 ppm) may be obtained by decreasing the resonance ejection scan rate of the instrument. However, this is achieved at the cost an increase in the time required for data acquisition [17]. Alternatively, ion trap mass spectrometers may be coupled with high resolution mass analyzers such as TOF [31], FT-ICR [32], or the Orbitrap [33].

1.4.2 Charge State Manipulation

McLuckey and colleagues have developed a method that utilizes gas-phase ion/ion proton transfer reactions to reduce the charge states of multiply charged product ions to their singly charged forms, thereby readily enabling the determination of their charges, and thus masses, and reducing the need for high resolution instrumentation. The general form of a proton transfer reaction is

$$[M + nH]^{n+} + A^- \rightarrow [M + (n-1)H]^{(n-1)+} + AH$$

Sequential proton transfer reactions may reduce the final products to their singly $[M + H]^+$ charged forms. Ion/ion reactions can also be useful to reduce mixture complexity by separating ions that have the same m/z, but different mass and charge. Ion/ion proton reactions can be performed both externally and internally to the mass spectrometer. External ion/ion reactions are advantageous as they can be used with almost any type of mass analyzer [34]. Ion/ion reactions inside the mass spectrometer have primarily been performed in ion traps, which have the advantage of being able to employ ion/ion reactions within the context of multistage mass spectrometry experiments [35, 36].

In addition to product ion charge state manipulations, it is also possible to manipulate the precursor ion charge state. This is useful in protein mixture analyses to concentrate and charge state purify precursor ion populations in the gas phase prior to subsequent fragmentation [37-39]. Since ions in an ion trap have frequencies of motion that are dependent on m/z, ion/ion proton transfer reaction rates for given m/z window can be inhibited in a selective manner via the application of a single-frequency on-resonance (SFOR) low amplitude ac signal with the ion of interest. This technique, known as ion parking, 'parks' selected ions within a narrow m/z range, while ions that are not in the specified m/z window continue to undergo proton transfer reactions [40]. A related technique termed 'parallel ion parking', uses a tailored waveform that contains two or more discrete frequencies such that ions over a range of m/z values can be parked simultaneously (non-selective ion parking) [41]. Due to the increase in m/z ratio that results from a decrease in charge, ion/ion reactions may require the ability to extend the mass range of the instrument. To date this has only been possible with 'home built' ion trap instrumentation that allow modification of the operating software. However, a new

approach known as HALF parallel parking, enabled by the application of high amplitude, low frequency broadband auxiliary ac signal, slows down the ion/ion reaction rates over a broader m/z region [42]. By manipulation of the frequency and amplitude of this voltage, the m/z range affected can be adjusted so that charge reduced product ions are maintained within a mass range that is accessible on commercially available ion trap mass spectrometry instrumentation.

1.5 Sequence Information

Another potential issue limiting top down proteomics is that of acquiring sufficient fragmentation of the intact protein ion to allow for detailed sequence information to be obtained in order to subsequently identify and characterize the protein. Similar to that for peptide ion dissociation, the sites and extent of fragmentation observed is highly dependent on the amino acid sequence and charge state (i.e., proton mobility) of the protein precursor ion. Thus, if the available fragmentation energy is predominantly directed towards the cleavage of certain bonds, limited sequence information will be obtained. There are currently three solutions to this issue: 1) fragmenting multiple precursor ion charge states to obtain complementary sequence information, 2) performing multiple stages (MS^n) of dissociation on a given precursor ion charge state to obtain additional sequence information, and 3) using alternative dissociation chemistries, such as electron capture dissociation (ECD) or electron transfer dissociation (ETD).

It is possible to extend the sequence coverage obtained and subsequently to obtain more detailed structural information for protein characterization by performing tandem mass spectrometry on different charge states of a protein. As seen for peptide ion

dissociation, the fragmentation of low protein precursor ion charge states, where the number of ionizing protons $\leq$ the number of arginine residues (i.e., non-mobile protons) commonly give rise to the loss of small molecules or exhibit enhanced fragmentation at the C-terminal side of aspartic acid. The formation of these enhanced product ions has been rationalized as being due to the high proton affinity of the arginine side chain sequestering the ionizing protons, thereby causing the fragmentation reactions to proceed via 'charge localized' (i.e. enhanced losses of NH_3 from the arginine side chains) or 'charge remote' (i.e., enhanced C-terminal aspartic acid cleavage) fragmentation mechanisms [43]. High charge state precursor ions, where the number of ionizing protons > the combined number of arginine, lysine and histidine residues (i.e., mobile protons), tend to exhibit enhanced fragmentation at the N-terminal side of proline residues, presumably via 'charge localized' reaction mechanisms resulting from the high local proton affinity of the proline imide bond. Dissociation of intermediate charge states (i.e., partially mobile protons) typically result in relatively non-specific fragmentation of the backbone [44]. Thus, by fragmenting charge states that are representative of each of these 'proton mobility' classes (i.e., mobile, partially mobile and non-mobile), it is possible to obtain more extensive sequence coverage than that observed by dissociation of only a single charge state [17]. The utility of this approach will be discussed in more detail in Chapter 3 of this thesis.

Alternatively, multiple stages of dissociation (e.g., MS^3) may be employed to obtain more extensive sequence information [43, 45, 46]. For example, when the initial MS/MS fragmentation results in the formation of only a handful of dominant product ions, further dissociation of a selected precursor ion, that may have a different charge

state (discussed above) and structure compared to its precursor ion, may allow access to different fragmentation channels, and the subsequent formation of further structural information. The utility of this approach will also be discussed in more detail in Chapter 3 of this thesis.

In the majority of cases, protein ions do not fragment sufficiently by collision induced dissociation (CID) to give complete sequence information. However, alternative dissociation techniques, such as electron capture dissociation (ECD) [47, 48], used in high resolution FT-ICR mass spectrometry, and electron transfer dissociation (ETD) [49], used in ion traps, may provide complementary or more extensive sequence information, particularly for the characterization of post translationally modified proteins. In contrast to collision induced dissociation that leads to the formation of b- and y-type product ions via cleavage of C-N amide bonds along the protein backbone, ECD and ETD lead to the formation of c- and z-type ions via cleavage of N-Cα bonds, as illustrated in Scheme 1.1. These techniques therefore provide an additional mode of dissociation for large multiply charged intact protein ions. ECD involves the capture of an electron with near thermal energy by multiply charged $[M+nH]^{n+}$ protein ions to yield odd electron reduced $[M+nH]^{(n-1)+\bullet}$ products. This process is exothermic and provides the energy required for fragmentation of the protein backbone. The mechanism for ECD has been proposed to involve the release of a high energy $H^{\bullet}$ in the initial reduction step, which may be collisionally de-excited and captured by a functional group within the protein ion, which then undergoes fragmentation through a nonergodic energy deposition process, quite distinctive from CID and other related dissociative "heating" techniques. ETD occurs via the gas-phase reaction of multiply protonated protein ions with anions of low electron

affinity, resulting in electron transfer to the positively charged protein ion [49]. After electron transfer, the charge reduced-peptide ion dissociates through the same mechanisms believed to responsible for ECD. Both of these dissociation techniques provide extensive backbone dissociation that is indifferent to either the sequence or the presence of labile PTMs, thus allowing for high sequence coverage and the possibility that labile modifications will remain intact. However, both ECD and ETD can suffer from sequential electron capture or electron transfer reactions of the products, which can lead to neutralization of product ions as well as the production of internal fragment ions. To inhibit this type of fragmentation, a variation of the parallel ion parking method based on parking all first generation product ions whose m/z varies significantly from the reactants was recently developed [50]. This technique utilizes a filtered noise field (FNF) waveform where notches in the waveform allow for the uninhibited reaction of selected analyte cations and reagent anions while all products differing in m/z from the reactant ions undergo inhibition of their ion/ion reaction rates and are thus 'parked'.

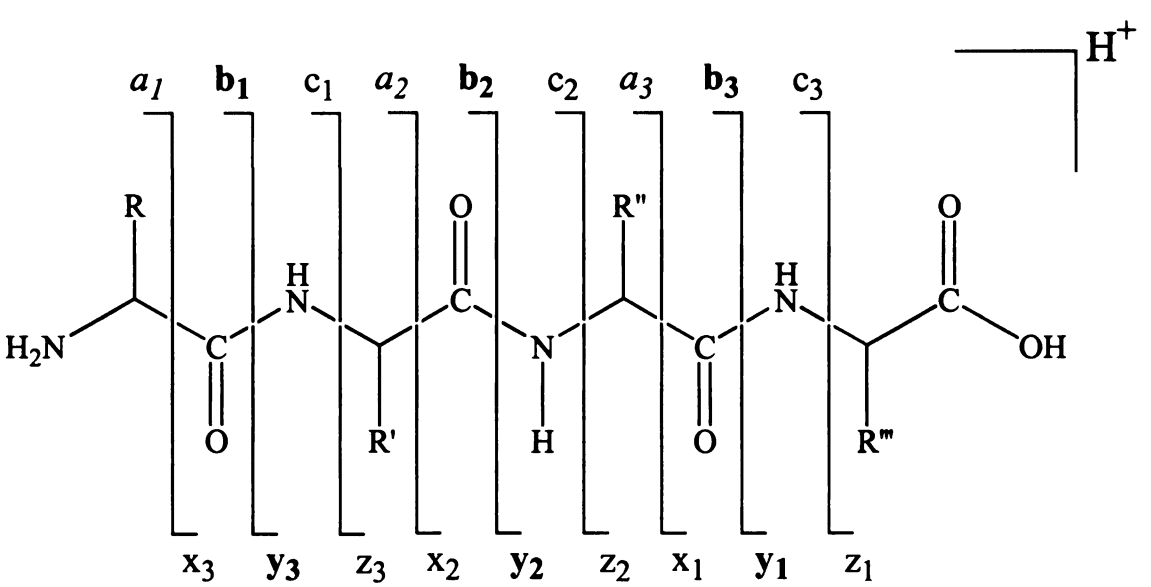

Scheme 1.1 Nomenclature for protein (and peptide) fragment ions.

1.6 Software/Database Analysis

The availability of bioinformatic tools for the analysis and data interrogation of product ion spectra derived from top down mass spectrometry analysis currently lag behind those available for peptide based bottom up analysis. Although the fragmentation of peptide ions have been extensively studied in a variety of tandem mass spectrometers and under a wide range of conditions, the fragmentation of whole protein ions is a relatively new technique and thus has received less attention. Our understanding of the factors that influence the dissociation of intact protein ions, while improving, is not complete, potentially limiting the utility of top down approaches for automated high throughput analysis [21]. Preliminary studies have indicated that protein fragmentation follows similar 'rules' to peptide fragmentation, as mentioned in Section 1.5. However, further studies examining the influence of charge state, proton mobility, sequence, and conformation on the observed fragmentation pathways and relative abundances of the resultant product ions would aid additional advances in the field.

Currently, the most extensively developed tools for protein identification and characterization based on interrogation of 'top down' protein product ion spectra are Thrash and ProSight PTM (https://prosightptm.scs.uiuc.edu/), described by Horn [51] and Kelleher *et. al.* [52], respectively. Thrash can be used for the automatic reduction and interpretation of high resolution data obtained from the electrospray ionization of large molecules. It identifies isotopic clusters, resolves those that overlap, and subjects these to an automated charge determination algorithm and to an isotopic abundance distribution-fitting algorithm. Alternatively, ion/ion reactions, as discussed in section 1.4.2, can be used to reduce multiply charged product ions to their singly charged forms, thereby

greatly simplifying the interpretation of the spectra [37]. Once the product ion masses have been obtained they can be compared against the available sequence databases by using database search algorithms [37, 38, 53]. For example, ProSight PTM [22, 52] allows for probability-based protein identifications based on top down data where the list of possible sequences is given with several different scores, while a second scoring algorithm, called the McLuckey score, also includes the ability to weight the score to account for cleavages at known preferential fragmentation sites [37, 39], by taking into account the abundances of each of the product ions observed.

1.7 Aims of this Thesis

The aims of this thesis are:

1. to examine the gas-phase fragmentation reactions of a series of site-directed mutagenesis products of *Staphylococcus aureus* dihydroneopterin aldolase (SaDHNA) by multistage tandem mass spectrometry (MS/MS and MS^3) in a linear quadrupole ion trap in order to determine the utility of this instrumentation for routine 'top down' recombinant protein characterization,
2. to explore the effect of single amino acid mutations and the potential role of protein structure on the charge state dependent gas-phase fragmentation behavior of intact protein ions, and;

3. to characterize the products of the reactions of (a) the WT SaDHNA and (b) the Y61F site-directed mutatgenesis product of SaDHNA with the substrate DHNP and to determine the structure-function role of the tyrosine residue within the active site.

CHAPTER TWO

Experimental

2.1 Materials

Methanol (HPLC grade) and ubiquitin (from bovine red blood cells) were purchased from Sigma-Aldrich (St. Louis, MO, USA). Glacial acetic acid (ACS grade) was purchased from Spectrum Chemicals (Gardena, CA, USA). 7,8-dihydro-D-neopterin (DHNP), 6-hydroxymethyl-7,8-dihydropterin (HP), 7,8-dihydroxanthopterin (DHXP), 6-formyl-7,8-dihydropterin (FDHP), and 6-hydroxymethylpterin (HPO) were purchased from Schircks Laboratories. Other molecular biology reagents were purchased from New England Biolab. All solutions were prepared using deionized water purified by a Barnstead nanopure diamond purification system (Dubuque, Iowa, USA). All reagents were used as supplied without further purification.

2.2 Site-directed Mutagenesis and Protein Purification

The SaDHNA proteins were prepared by Ms. Yi Wang within the Department of Biochemistry and Molecular Biology at Michigan State University [54]. Briefly, the SaDHNA gene, as well as those for the SaDHNA site-directed mutants, were cloned into a home-made prokaryotic expression vector (pET17H) by PCR from *S. aureus* genomic DNA. The verified expression constructs were then transformed into *E. coli* strain BL21(DE3)pLysS for over-production of the SaDHNA or mutant protein. Following induction of SaDHNA production, *E. coli* cells were lysed and purified by Ni-NTA (Qiagen) column and Bio-Gel A-0.5m gel column (Bio-Rad) chromatography. Pure

SaDHNA fractions were pooled, concentrated, dialyzed against 5 mM TrisHCl (pH 8.0), lyophilized, and stored at -80 °C.

The amino acid sequence for the WT SaDHNA protein is shown in Scheme 2.1. The sequences of the individual site-directed mutagenesis products of SaDHNA (E29A, Y61F, Y61A, E81A, K107A, and K107Q) are shown in Scheme 2.1 by the amino acids listed in the boxed regions below the WT sequence. The N-terminal six histidine residues were engineered to facilitate purification of the protein. Therefore, the amino acid numbering used here differs by seven residues relative to the native protein.

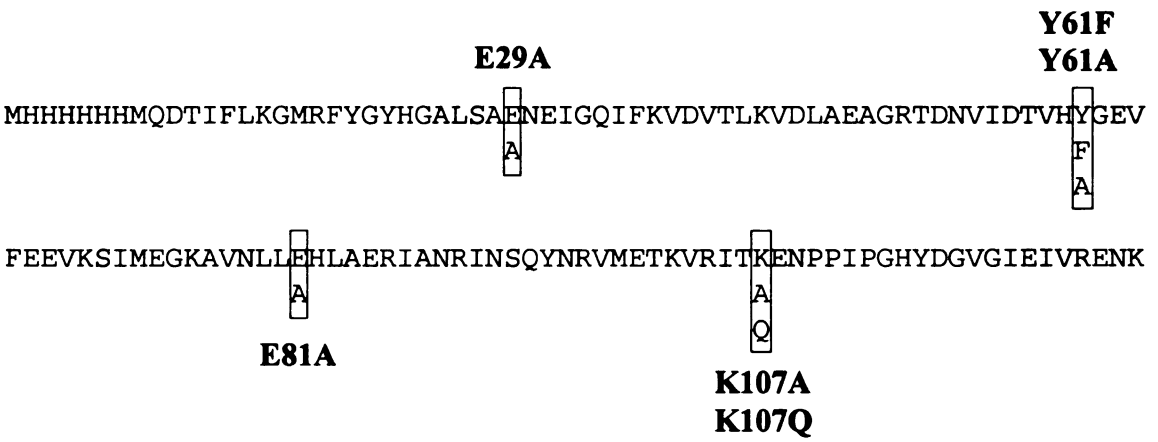

Scheme 2.1 Amino acid sequence of the WT SaDHNA protein. The site of modification for each of the site-directed mutants is shown in boxed regions.

2.3 Mass Spectrometry

2.3.1 Intact Mass Analysis of the WT SaDHNA Protein and its Site-directed Mutants by High Resolution FT-ICR Mass Spectrometry

Accurate molecular weight experiments were performed on a Bruker Apex III 7.0 Tesla Fourier transform ion cyclotron resonance (FT-ICR) mass spectrometer (Billercia, MA). A 6 point external calibration was performed, whereby the 6^{th} isotopic peaks from

the $[M+8H]^{8+}$ to $[M+13H]^{13+}$ charge states of bovine ubiquitin were experimentally determined and linearly fitted against the theoretical values by the FT-ICR software Xmass version 6.0.3. Both the ubiquitin calibration standard and the SaDHNA proteins were dissolved in aqueous methanol/water/acetic acid (50:49:1) at concentrations of ~ 10 pmol/μL, then introduced to the mass spectrometer via a syringe pump at a flow rate of 120 μL/hr by electrospray ionization (ESI). All MS spectra were obtained in broadband mode (120 scans, 1 M data points, m/z 200-2000). Experimental molecular weights for the SaDHNA proteins were calculated based on the 10^{th} isotopic peak (typically the most abundant) from the $[M+18H]^{18+}$ charge state. Theoretical isotopic distributions were calculated by IsoPro version 3.0. The reported mass accuracies (ppm) are based on the theoretical and experimental neutral molecular weights for the 10^{th} isotopic peak. Resolution calculations were performed by the FT-ICR software Xmass version 6.0.3.

2.3.2 Multistage Tandem Mass Spectrometry Characterization of the WT SaDHNA Protein and its Site-directed Mutants by Linear Quadrupole Ion Trap Mass Spectrometry

Experiments were performed using a Thermo model LTQ linear ion trap mass spectrometer (San Jose, CA). The WT SaDHNA protein was dissolved in either aqueous methanol/water/acetic acid (50:49:1) (to form charge states ranging from $[M+12H]^{12+}$ to $[M+24H]^{24+}$) or water (to form charge states ranging from $[M+8H]^{8+}$ to $[M+15H]^{15+}$) at concentrations of ~1 pmol/μL. All of the mutant proteins were dissolved in aqueous methanol/water/acetic acid (50:49:1). Protein solutions were then introduced to the mass spectrometer at a flow rate of 0.5 μL/min by nanoelectrospray ionization (nESI). The

nESI conditions were optimized to maximize the intensity of the multiply protonated precursor ions of the SaDHNA proteins and to minimize adduction. Typical nESI conditions under methanol/water/acetic acid (50:49:1) conditions were: spray voltage 1.8 kV, heated capillary temperature 325 °C (the heated capillary was operated at this temperature in order to minimize the appearance of non-covalent adduct peaks), capillary voltage -60 V, and tube lens voltage -100 V. Typical nESI conditions under aqueous conditions were: spray voltage 1.8 kV, heated capillary temperature 300 °C, capillary voltage -100 V, and tube lens voltage -250 V. CID MS/MS and MS^3 spectra were acquired at an activation q value of 0.25 using an isolation width of 2 Da, a normalized collision energy of 30%, and an activation time of 30 ms. The precursor ion accumulation time for each scan was controlled by the automatic gain control (AGC) function of the instrument in order to maintain an ion target number of 1000 (arbitrary value) during MS/MS and MS^3 experiments. Mass spectra were acquired using the 'normal' (16,000 u/s), 'enhanced' (experimentally determined as 4,400 u/s), 'zoom' (1,100 u/s), and 'ultrazoom' (28 u/s) resonance ejection scan modes of the linear ion trap mass spectrometer. The MS/MS product ion spectra shown were the average of 250, 500, and 500 individual mass analysis scans for 'enhanced', 'zoom', and 'ultrazoom' resonance ejection scan modes, respectively. MS^3 product ion spectra were the average of 500, 1000, and 500 individual mass analysis scans for 'enhanced', 'zoom', and 'ultrazoom' resonance ejection scan modes, respectively. A five point Gaussian smoothing was applied prior to interpretation of the MS/MS and MS^3 product ion spectra. Product ion assignments were restricted to b-type and y-type ions.

Cleavage intensity ratio (CIR) calculations [55] were performed for the fragmentation of the WT SaDHNA protein according to the following equation:

$$CIR_s = \frac{\sum_{z=1}^{z} b_s^{z+} + y_s^{z+}}{\frac{1}{N}\sum_{i=1}^{N}\sum_{z=1}^{Z}\left(b_i^{z+} + y_i^{z+}\right)} \quad (19)$$

where N is the number of cleavage sites, s is the cleavage site of interest ($1 \leq s \leq N$), z is the charge state of the product ions, and b_i^{z+} and y_i^{z+} are the normalized intensities of the b- and y-type ions with z charge at the ith cleavage. The intensity of each ion was normalized by dividing by the square root of its charge (z).

2.3.3 Characterization of the Products Formed by the Reaction of DHNP with the WT and Y61F SaDHNA Proteins by Linear Quadrupole Ion Trap Mass Spectrometry

Enzymatic reactions were performed using 300 µl samples contained 200 µM 7,8-dihydroneopterin and 4 µM WT SaDHNA or 10 µM Y61F SaDHNA in 5 mM ammonium carbonate, pH 8. 20 µL aliquots of the reaction mixtures were taken at 1-min intervals and mixed with 80 µL of an aqueous methanol/water/acetic acid (50:49:1) solution to quench the reaction. The samples were then further diluted with the same solution and introduced to a Thermo model LTQ linear ion trap mass spectrometer (San Jose, CA) at a flow rate of 0.5 µL/min by nanoelectrospray ionization (nESI). The nESI conditions used were: spray voltage 1.8 kV, heated capillary temperature 200 °C,

capillary voltage -10 V, and tube lens voltage -50 V. CID MS/MS and MS^3 spectra were acquired at an activation q value of 0.25 using an isolation width of 1 or 2 Da (to monoisotopically isolate the precursor ion), a normalized collision energy of 30 - 40%, and an activation time of 30 ms or 300 ms. The values were chosen such that the gentlest conditions were used in order to completely dissociate the selected precursor ion (i.e. some precursor ions required a larger normalized collision energy and/or longer activation time). The MS/MS and MS^3 product ion spectra shown are the average of 60 individual mass analysis scans in the 'enhanced' resonance ejection scan mode of the linear ion trap mass spectrometer. All product ion assignments were performed by manual inspection of the spectrum.

CHAPTER THREE

Top Down Characterization of *Staphylococcus aureus* Dihydroneopterin Aldolase and its Site-directed Mutagenesis Products*

3.1 Introduction

A particular attraction of the top down approach for protein characterization when using the quadrupole ion trap is the capacity to perform multiple stages of dissociation (e.g., MS^3), in order to extend the sequence coverage that can be obtained from a protein ion of interest, [43] or to obtain more detailed characterization of any protein modifications that may be present [45, 46]. To date, however, the limited commercial availability of ion trap instrumentation with ion/ion reaction capabilities for charge state determination has hampered the widespread implementation of this approach. In the absence of ion/ion reactions in the ion trap, the upper limit to the mass of a protein from which the charge states of its multiply charged product ions can be determined is defined by the resolution that can be obtained during mass analysis. Quadrupole ion trap mass spectrometers are generally operated under conditions that yield relatively low resolution mass analyzer performance, in order to minimize the time required for acquisition of the mass spectrum, and thereby maximize the data acquisition rate.

---

* The results described in this Chapter have been published in: Scherperel, G.; Yan, H.; Wang, Y. and Reid, G. E. 'Top down' characterization of site-directed mutagenesis products of Staphylococcus aureus dihydroneopterin aldolase by multistage tandem mass spectrometry in a linear quadrupole ion trap. *The Analyst* **2006**, *131*, 291-302.

However, as discussed in section 1.2.2.1 of Chapter 1, mass analyzer resolution in the ion trap is inversely proportional to the scan rate employed for resonance ejection of ions for mass analysis. Thus, high resolution performance may be obtained by simply decreasing the resonance ejection scan rate of the instrument. Although decreased resonance ejection scan rates are accompanied by a proportionate increase in the data acquisition time, this is potentially offset by a concurrent increase in the sequence information that may be obtained upon interpretation of the resultant high resolution data. The ability to obtain high resolution mass analysis in the quadrupole ion trap is also limited by the finite ion storage capacity of the instrumentation, due to increased space charge effects observed at higher charge densities of stored ions.

Here, the intact masses of the wild type (WT) *Staphylococcus aureus* dihydroneopterin aldolase (SaDHNA) and a series of site-directed mutagenesis products from it were determined using FT-ICR mass spectrometry. Then, the gas-phase fragmentation reactions of these proteins were examined by multistage tandem mass spectrometry (MS/MS and MS^3) in a linear quadrupole ion trap, in order to evaluate the utility of this instrumentation for routine top down recombinant protein characterization, as well as to further extend the current state of knowledge regarding the sequence and charge state dependence to the gas-phase fragmentation reactions of intact multiply charged protein ions.

3.2 Analysis of SaDHNA Mutants by High Resolution FT-ICR Mass Spectrometry

The intact masses of the WT SaDHNA protein and its Y61A, Y61F, E29A, E81A, K100A, and K100Q site-directed mutagenesis products were obtained by FT-ICR mass

spectrometry and are show in Table 3.1. The experimental molecular weights and resolution for each protein were calculated as described in section 2.3.1 of Chapter 2. In each case, the experimentally determined masses were consistent to within less than 5 ppm with those calculated from the amino acid sequence. Determination of the intact masses alone, however, does not provide confirmation that the site-directed mutagenesis products actually correspond to the expected mutations, nor that the mutations are present at the expected positions within the amino acid sequence. For example, the E29A site-directed mutagenesis product has the same experimentally determined mass (to within 7 ppm) as that of the E81A site-directed mutagenesis product. Furthermore, the calculated mass difference of 58 Da between the WT SaDHNA protein and the E29A or E81A site-directed mutagenesis product could result from substitution of an alanine residue at any of the thirteen glutamic acid residues within the sequence, or from substitution of a glycine residue at any of the six aspartic acid residues (although not present within the SaDHNA sequence, substitution of tryptophan to glutamine would also give rise to a mass difference of 58 Da). Thus, in order to further characterize these proteins, tandem mass spectrometry was performed in a linear ion trap.

3.3 Optimization of Linear Ion Trap Conditions for Top Down Work

The effect of resonance ejection scan rate, ion target number, and the number of scans acquired for a product ion spectrum must all be considered in order to enable the development of robust top down methods for recombinant protein characterization using the linear quadrupole ion trap mass spectrometer. Each of these are examined in more detail below, using product ion spectra obtained from the dissociation of multiply

protonated ubiquitin or from the dissociation of the multiply protonated wild type WT SaDHNA protein.

Table 3.1 Intact molecular weights for the WT and mutant SaDHNA proteins obtained by high resolution FT-ICR mass spectrometry.

	Calculated MW (Da)	Experimental MW* (Da)	Mass Accuracy (ppm)	Resolution (FWHM)
WT	14688.4653	14688.50724	2.9	72,387
Y61F	14672.47032	14672.50524	2.4	72,353
Y61A	14596.43904	14596.47324	2.3	72,043
E29A	14630.45976	14630.51304	3.6	72,890
E81A	14630.45976	14630.40504	-3.7	71,036
K107A	14631.40728	14631.47244	4.6	73,328
K107Q	14688.42876	14688.37044	-4.0	69,167

* $[M+18H]^{18+}$

3.3.1 Resonance Ejection Scan Rate

As discussed in section 1.2.2.1 of Chapter 1, the resolution obtained in an ion trap mass spectrometer is inversely proportional to the resonance ejection scan rate of the instrument. Thus, a slower scan rate will yield better resolution, however, it will also increase the data acquisition time and decrease the sensitivity. It is therefore necessary to choose a scan rate that provides a good compromise between resolution, sensitivity, and data acquisition time. The software of the linear ion trap employed for these studies allows for resonance ejection scan rates of 16,000 u/sec ('normal'), 4,400 u/sec

('enhanced'), 1,100 u/sec ('zoom'), and 28 u/sec ('ultrazoom'). The slowest scan rate allows for the highest resolution, but the worst sensitivity and the longest acquisition time. The fastest scan rate gives the lowest resolution, but the best sensitivity and the shortest acquisition time. The difference in the resolution obtained from 'enhanced', 'zoom', and 'ultrazoom' resonance ejection scans are illustrated in Figure 3.1 for analysis of the b_{31}^{5+} product ion from dissociation of the $[M + 20H]^{20+}$ charge state of the WT SaDHNA protein. Poor resolution is seen for the 'enhanced' spectra (Figure 3.1A). The 'zoom' scan spectrum (Figure 3.1B) provides adequate resolution (4132) for charge state determination, but still does not fully resolve the isotopic distribution. The 'ultrazoom' scan (Figure 3.1C) provides highest resolution, determined to be 9,415.

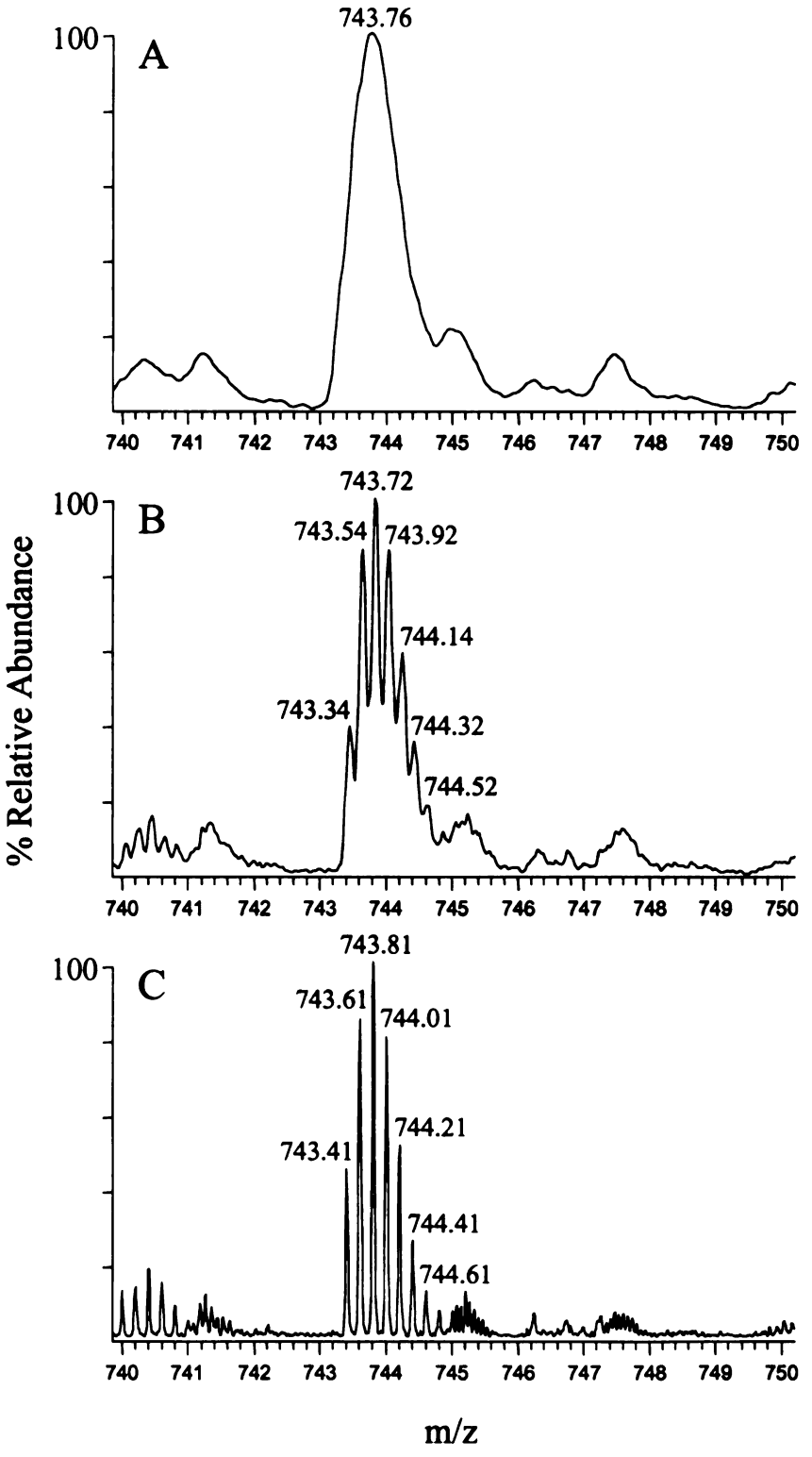

Figure 3.1 Effect of resonance ejection scan rate on resolution. CID MS/MS product ion spectrum (b_{31}^{5+}) of the $[M + 20H]^{20+}$ ion from the WT SaDHNA in (A) 'enhanced' mode, (B) 'zoom' mode, and (C) 'ultrazoom' mode.

3.3.2 Target Number

The ion 'target' number, or the number of ions allowed into the trap, is another important parameter to be considered when performing top down experiments in a linear ion trap. This is controlled by the automatic gain control (AGC) function of the instrument. In order to minimize the time required for data acquisition, as well as to improve the signal-to-noise ratio of the resultant product ion spectra, it would be beneficial to increase the number of ions that are isolated in the ion trap for dissociation. However, an increased number of ions in the trap leads to a proportionate decrease in the resolution of the resultant product ion spectrum due to increased space charge effects during resonance ejection. The effect of target number on resolution is shown in Figure 3.2 for analysis of the y_{58}^{9+} product ion from dissociation of the $[M + 11H]^{11+}$ precursor ion charge state of ubiquitin. Here it can be see that a high target number (10,000) yields little to no resolution of the isotopic distribution (Figure 3.2A). A medium 'target' number (2,500) provides the resolution needed to identify the charge state of the product ion, but 'local' space charge effects can still be observed for the first few isotopes (Figure 3.2B). It can be seen from Figure 3.2C that the best resolution is obtained at the lowest target number (500).

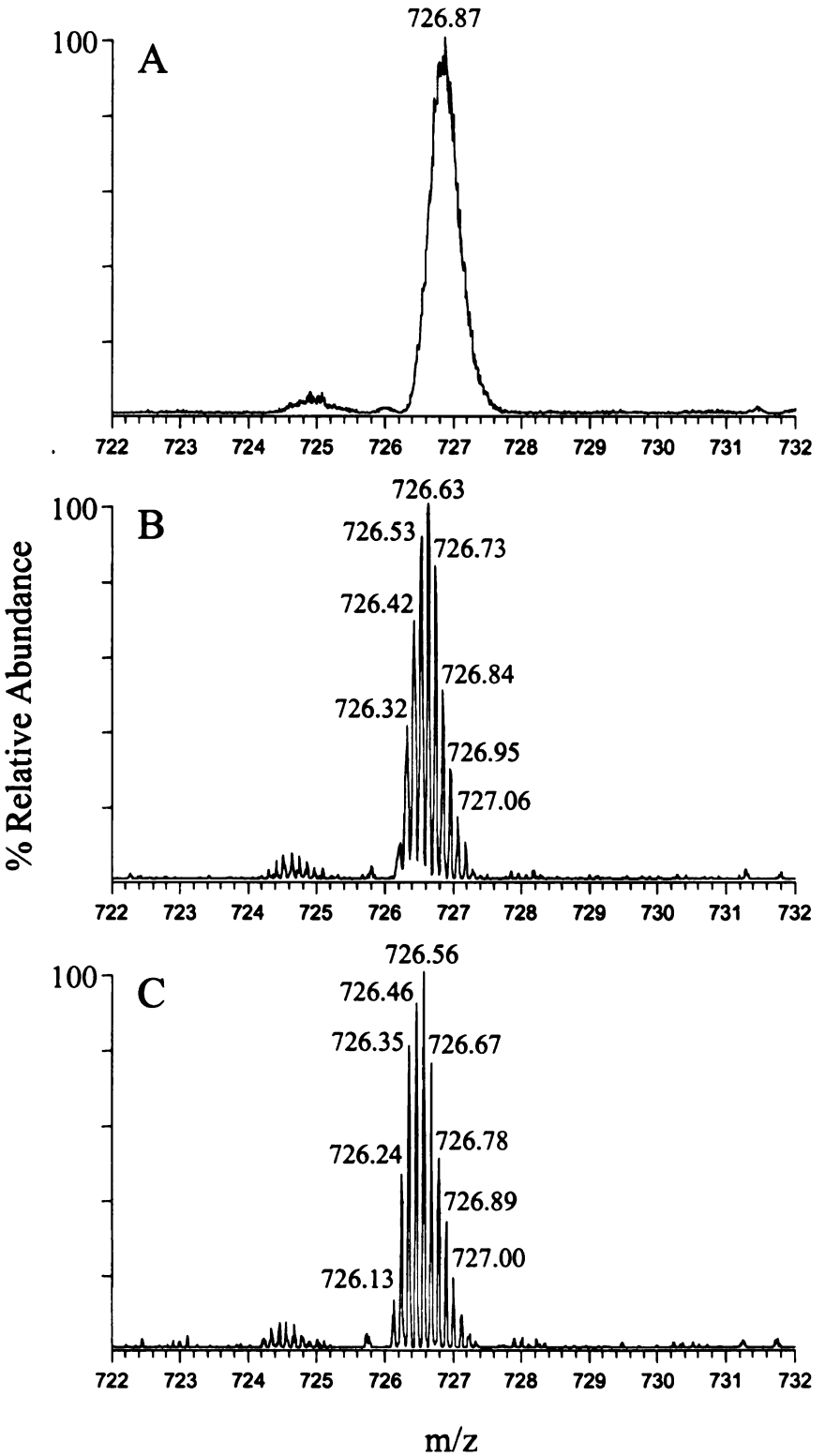

Figure 3.2 Effect of ion 'target' number on resolution. 'Ultrazoom' scan mode CID MS/MS product ion spectrum (y_{58}^{9+}) of the $[M + 11H]^{11+}$ ion from ubiquitin with a target number of (A) 10,000, (B) 2500, and (C) 500.

3.3.3 Scan Number

Lastly, the number of scans that are averaged together must be optimized. Although it is desirable to acquire a high number of scans for good signal averaging (better signal-to-noise (S/N) ratio and peak shapes), a low number of scans is desired to increase the duty cycle of the experiment. The S/N ratio increases with the square root of the number of scans taken. In Figure 3.3A, 100 'enhanced' mode scans were acquired in 0.8 minutes, while in Figure 3.3B 1,000 'enhanced' mode scans were acquired over approximately 8 minutes. Thus, the S/N ratio could be increased by a factor of about 3.3 by increasing the number of scans by a factor of ten. Eventually a point is reached where the improvement in the signal-to-noise ratio achieved by averaging more scans does not outweigh the increase in acquisition time.

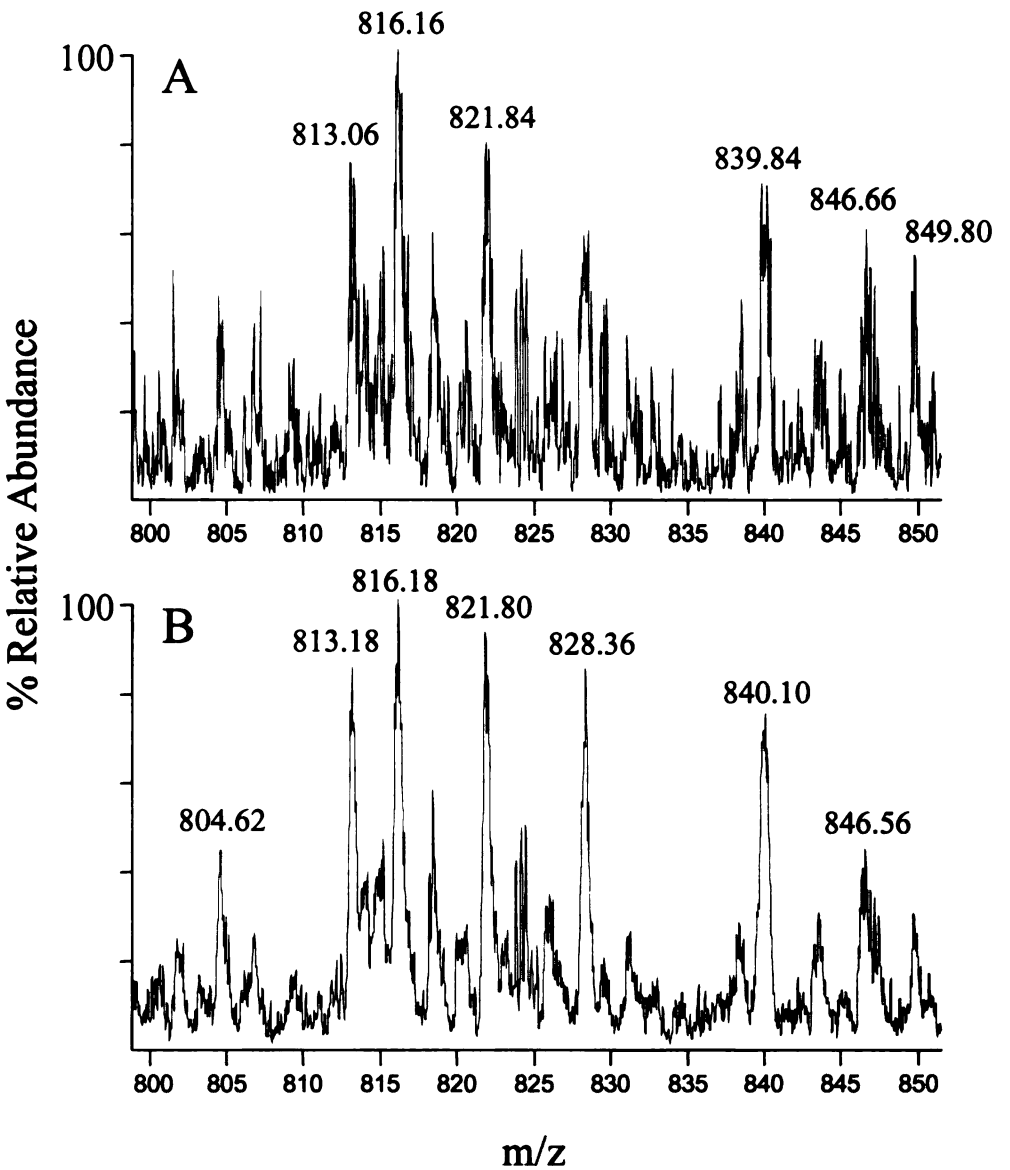

Figure 3.3 Effect of scan number on S/N ratio. 'Enhanced' scan mode CID MS/MS product ion spectrum of the $[M + 11H]^{11+}$ ion from ubiquitin obtained with a scan number of (A) 100 and (B) 1000.

3.3.4 Optimized Conditions for Routine Top Down Analysis of Recombinant Proteins of Moderate Mass in the Linear Quadrupole Ion Trap

Based on the results from the experiments discussed above, the following conditions were used for all subsequent experiments. The ion target number was set at 1000 for all MS/MS and MS^3 experiments. The MS/MS product ion spectra shown were the average of 250, 500, and 500 individual mass analysis scans for 'enhanced', 'zoom', and 'ultrazoom' resonance ejection scan modes, respectively. At a target number of 1000, 250 enhanced MS/MS scans takes approximately 2 minutes, 500 zoom MS/MS scans takes about 15 minutes, and 500 ultrazoom MS/MS scans takes about 30 minutes. MS^3 product ion spectra were the average of 500, 1000, and 500 individual mass analysis scans for 'enhanced', 'zoom', and 'ultrazoom' resonance ejection scan modes, respectively. At this target number, it takes roughly 5 minutes, 30 minutes, and 30 minutes, respectively, for these MS^3 scans.

3.4 Characterization of the WT SaDHNA protein

3.4.1 Examination of the CID MS/MS Fragmentation Behavior of the Multiply Protonated Precursor Ions Obtained by nESI from the WT SaDHNA Protein

As an initial step, mass spectra of the WT SaDHNA protein were acquired in order to observe the range of charge states produced by electrospray ionization that would then be amenable to subsequent dissociation by MS/MS (Figure 3.4). To obtain evidence to confirm the amino acid sequence of the WT SaDHNA protein, as well as to confirm that the mass differences obtained by FT-ICR associated with each of the site-directed mutagenesis products correspond to the expected mutations, product ion spectra

from selected precursor ion charge states of each protein were then obtained by CID MS/MS.

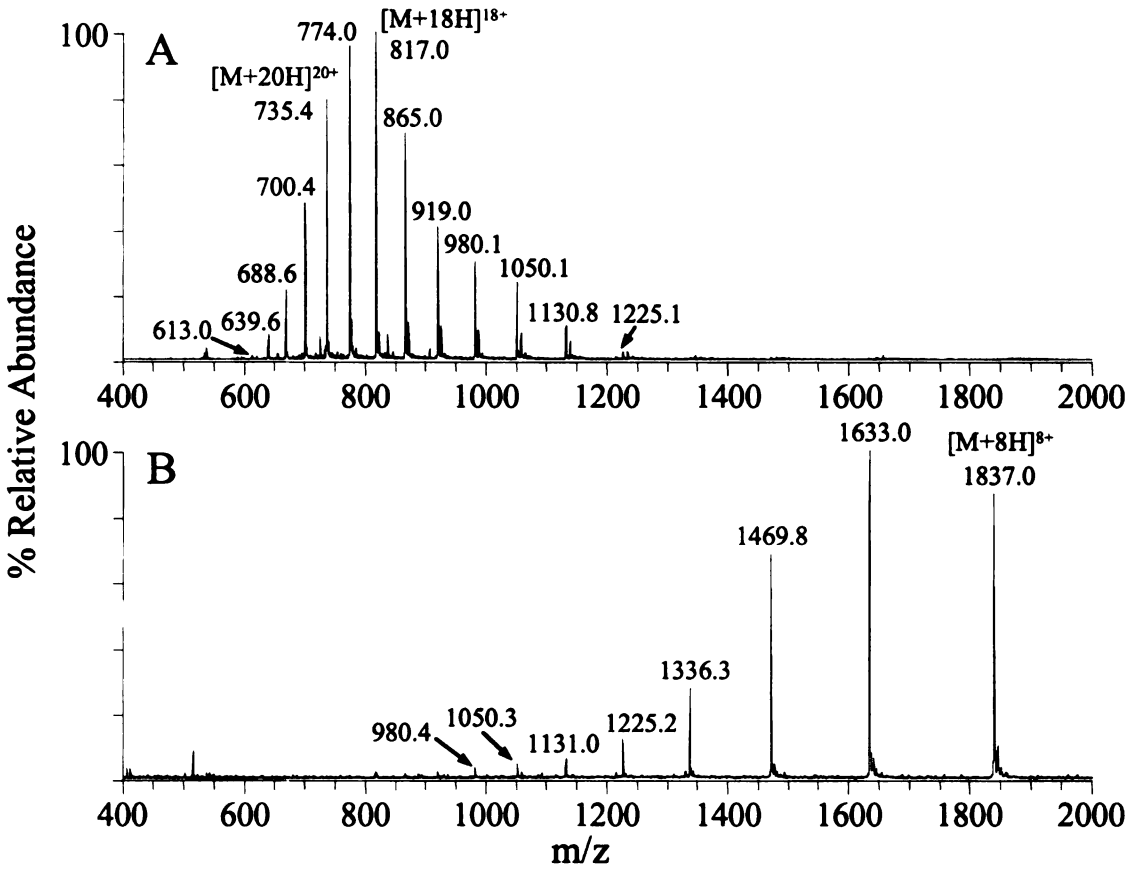

Figure 3.4 ESI MS of the WT SaDHNA protein. Charge states ranging from $[M+8H]^{8+}$ to $[M+24H]^{24+}$ were observed and characterized by CID MS/MS. (A) Methanol/Water/Acetic acid (50:49:1). (B) Water.

Within the experimental timescale required for protein characterization on a routine basis, it is typically not feasible to subject all of the precursor ion charge states that are observed by ESI to dissociation by CID MS/MS. However, it has been demonstrated previously that precursor ions within a certain charge state range often give rise to similar product ion spectra from which the same 'sequence' information can be obtained, whereas those from a different charge state range may give rise to product ion

spectra from which a different complementary set of 'sequence' information data can be derived [43, 56-58]. Therefore, from a practical standpoint, only a subset of the precursor ions that are formed by ESI need be selected for dissociation in order to observe essentially the full complement of 'sequence ions' that would be generated from dissociation of each of the protein precursor ion charge states. The major problem associated with this approach, however, is that it is difficult to predict *a priori* which of the available precursor ions for a given protein will give rise to product ion spectra that enable the desired sequence information to be obtained. Therefore, in order to initially determine the precursor ion charge states of the WT and site-directed mutagenesis products of SaDHNA that would be selected for dissociation and subsequent detailed structural characterization, a rapid survey of the gas-phase dissociation behavior of the WT protein was performed by subjecting each of the abundant precursor ion charge states from $[M + 8H]^{8+}$ (m/z 1837.0) to $[M + 22H]^{22+}$ (m/z 688.6) to CID MS/MS, with acquisition of the resultant product ion spectra using the 'low' resolution 'enhanced' resonance ejection MS/MS scan mode of the mass spectrometer. Product ion spectra with high signal-to- noise ratios were obtained in this mode of analysis by acquiring data from each charge state for approximately one minute each. For routine analyses, however, it is not practical to work with more than one set of conditions. Thus, the charge states obtained under the methanol/water/acetic acid conditions were focused on due to the more stable spray achieved under these conditions.

For the WT SaDHNA protein, dissociation of precursor ion charge states less than $[M + 19H]^{19+}$ led to the formation of spectra with large numbers of product ions from which extensive sequence information could be derived. In contrast, dissociation of the

$[M + 19H]^{19+}$ and higher precursor ion charge states resulted in the formation of spectra dominated by only a few product ions. Although these 'enhanced' scan mode MS/MS spectra were useful to evaluate the type and extent of fragmentation that occurred for each precursor ion charge state, this data was typically not useful for extensive characterization of the protein sequence, due to the inherent low resolution associated with the product ion spectra. Based on this initial survey, however, the $[M + 18H]^{18+}$ and $[M + 20H]^{20+}$ charge states, whose presence at high relative abundance enabled the acquisition of product ion spectra with good signal-to-noise ratios from a relatively low number of individual scans, were selected as being representative of the two main fragmentation behaviors. Further MS/MS product ion spectra were then acquired by using the 'zoom' and 'ultrazoom' resonance ejection scan modes for these two charge states.

The 'zoom' scan mode product ion spectra obtained by CID MS/MS of the $[M + 18H]^{18+}$ (m/z 817.0) and $[M + 20H]^{20+}$ (m/z 735.5) precursor ion charge states from the WT SaDHNA protein are shown in Figures 3.5A and 3.6A, respectively. For product ion spectra obtained using the 'ultrazoom' resonance ejection scan mode, only the regions of m/z where abundant product ions were observed (from m/z 650–1050) were acquired, due to the slow (28 u/s) scan rate associated with this scan mode, as well as a software limitation that restricted the acquisition of 'ultrazoom' data to 100 m/z wide regions of the mass spectrum. Each of the product ion spectra obtained by using the 'enhanced', 'zoom', and 'ultrazoom' resonance ejection scan modes for the +18 and +20 charge states were then manually interpreted, in order to determine the masses of the product ions in each spectrum that were sufficiently resolved to enable their charge state determination.

The identities of these experimentally determined masses were then assigned by comparison with the masses of the b- and y-type ions predicted from the SaDHNA sequence.

Due to the extensive fragmentation observed for the +18 charge state, the signal-to-noise ratio of the product ion spectrum shown in Figure 3.5A was significantly lower than that from the +20 charge state product ion spectrum shown in Figure 3.6A, even though the two precursor ions were initially present at similar relative abundances. Therefore, in order to obtain similar signal-to-noise ratios for these ions, the number of spectra acquired must be proportionate to the number of product ions that are formed. However, there is a practical limitation to the number of spectra that can be acquired within a reasonable timescale. For the 500 scans acquired here, analysis times of 15 minutes and 30 minutes respectively, were used for acquisition of the individual 'zoom' and 'ultrazoom' mass spectra. Although this seems quite long in comparison to that for acquisition of a product ion spectrum on a proteolytically derived peptide ion (typically a few seconds), it is important to note that when the time required for proteolytic digestion of the protein and chromatographic fractionation of the resultant peptide mixture is taken into account, the amount of 'sequence coverage per unit of time' that may be obtained by the top down approach is actually comparable to that obtained by the bottom up approach.

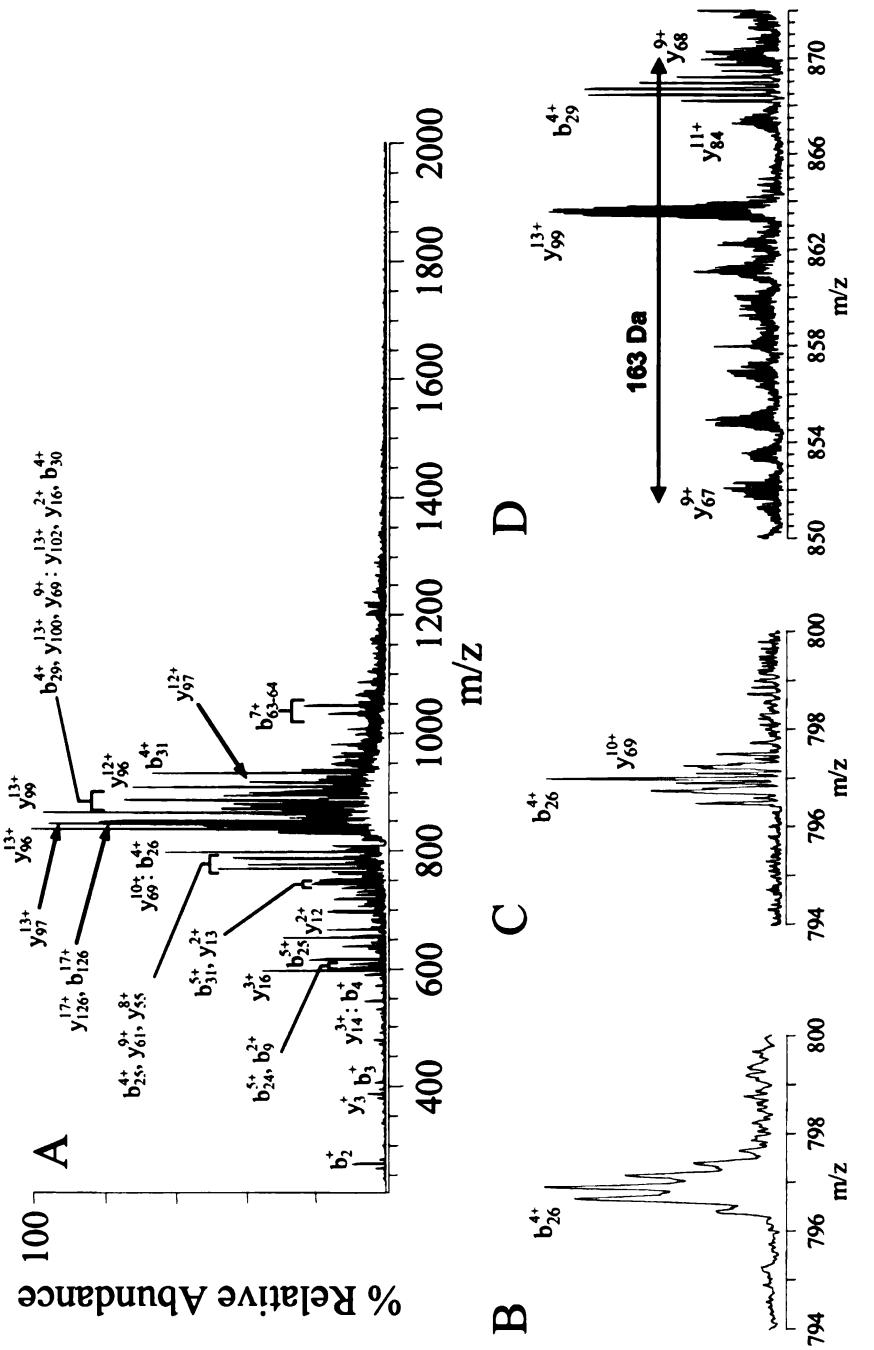

Figure 3.5 Multistage tandem mass spectrometry characterization of the $[M + 18H]^{18+}$ precursor ion charge state of the WT SaDHNA protein. (A) CID MS/MS product ion spectrum of the $[M + 18H]^{18+}$ ion acquired by resonance ejection in 'zoom' scan mode. (B) An expanded region of m/z from 794 to 800 from the 'zoom' scan, where only the b_{26}^{4+} product ion was identified. (C) The region of m/z from 794 to 800 acquired using an 'ultrazoom' resonance ejection scan, where b_{26}^{4+} and y_{69}^{10+} product ions were both observed. (D) The region of m/z from 850 to 872 acquired using an 'ultrazoom' resonance ejection scan.

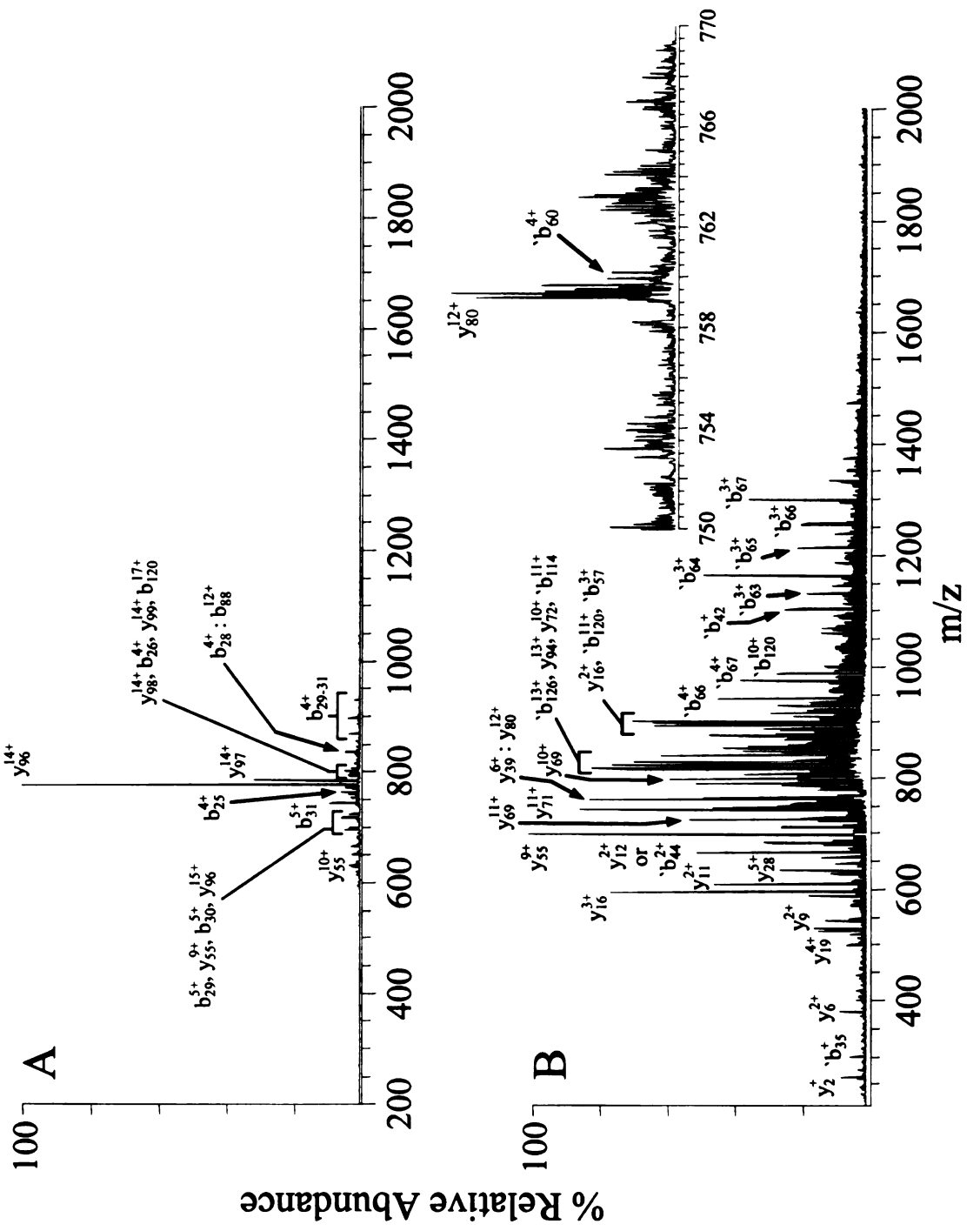

Figure 3.6 Multistage tandem mass spectrometry characterization of the $[M + 20H]^{20+}$ precursor ion charge state of the WT SaDHNA protein. (A) 'Zoom' scan mode CID MS/MS product ion spectrum of the $[M + 20H]^{20+}$ ion. (B) 'Zoom' scan mode CID MS^3 product ion spectrum of the y_{96}^{14+} ion obtained by MS/MS from the $[M + 20H]^{20+}$ ion in Figure 3.6A. The inset to Figure 3.6B shows the region of m/z from 750 to 770 acquired using an 'ultrazoom' resonance ejection scan.

The need to maintain high resolution also becomes increasingly important as the number of product ions formed by dissociation of a selected precursor ion increases, due to a greater probability that several product ions will be formed with different masses and charges but very similar m/z values. This is demonstrated in Figure 3.5B and C. Figure 3.5B shows the m/z 794 to 800 region of the 'zoom' scan MS/MS product ion spectrum obtained from the +18 charge state. The major ion observed in this region of the spectrum was identified as the b_{26}^{4+} product. However, based on the peak widths of the isotopes comprising this product ion, it was evident that there was at least one other ion present at an almost identical m/z ratio. Figure 3.5C shows the same region of m/z obtained from the 'ultrazoom' resonance ejection scan mode MS/MS product ion spectrum where two isotope distributions could be clearly resolved, thereby allowing the second product ion to be identified as the y_{69}^{10+} ion.

3.4.2 MS^3 Dissociation of the y_{96}^{14+} Product Ion Obtained by CID MS/ MS of the $[M + 20H]^{20+}$ Precursor Ion of the WT SaDHNA Protein

Since the ability to characterize a protein of interest by MS/MS is dictated by the extent of fragmentation that occurs along the peptide or protein backbone, if the fragmentation reactions are directed toward the formation of only a limited number of product ions, characterization of the peptide ion may not be possible. This is illustrated by the +20 charge state MS/MS data of the WT SaDHNA protein shown in Figure 3.6A where, due to formation of the dominant y_{96}^{14+} product ion, the number of amide bond cleavages that could be identified was significantly lower than that from the +18 charge state. However, given that the y_{96}^{14+} ion was formed at high relative abundance and

contains 75% of the protein sequence, this product ion is particularly suited to further dissociation by MS^3, thereby potentially allowing greater sequence information to be obtained. A further advantage of performing MS^3 on this ion is that the resolution required for identification of the resultant products was inherently lower, due to the lower mass and charge state of the y_{96}^{14+} ion compared to the intact +20 precursor ion.

The 'zoom' scan mode product ion spectrum obtained by MS^3 of the y_{96}^{14+} product ion from the +20 charge of the WT SaDHNA protein is shown in Figure 3.6B. Assignment of the extensive series of abundant product ion masses that were identified from the individual 'enhanced', 'zoom' and 'ultrazoom' resonance ejection scan mode MS^3 spectra for this ion enabled characterization of 14, 29, and 47 amide bond cleavage sites, respectively, with an overall sequence coverage of 44.9% for the intact protein (60.0% sequence coverage for the y_{96}^{14+} ion). Most of the b- and y-type ions that were observed in the MS/MS product ion spectra of the +20 charge state were also observed in the MS^3 spectra of the y_{96}^{14+} ion, with the obvious exception of those that corresponded to amide bond fragmentations between residues 1–32. However, additional product ions corresponding to a further 17 amide bond cleavages could be identified from the 'enhanced', 'zoom', and 'ultrazoom' MS^3 spectra, that were not observed from either the +18 or +20 charge state MS/MS product ion spectra. Note that while the numbering of the b-type ions shown in Figure 3.6B is the same as that used for the intact protein, in order to allow a direct comparison of the amide bond cleavages observed between MS/MS and MS^3 experiments, a superscript " ` " has been added to indicate their origin as 'internal' product ions from the y_{96}^{14+} precursor.

3.4.3 Sequence Coverage Obtained for the WT SaDHNA Protein

A summary of the amide bond cleavages identified and the percent sequence coverage obtained by interpretation of the individual 'enhanced', 'zoom', and 'ultrazoom' mode resonance ejection scan mode MS/MS and MS^3 product ion spectra from the +18 and +20 charge states of the WT SaDHNA protein are given in Table 3.2. It can be seen that product ions corresponding to the fragmentation of only 17 and 16 amide bonds along the protein backbone could be identified by interpretation of the 'enhanced' MS/MS product ion data from the +18 and +20 charge states respectively, primarily due to the low resolution associated with the this resonance ejection scan mode. In contrast, product ions corresponding to 30 and 36 amide bond fragmentations for the MS/MS of the +18 charge state, and 30 and 15 amide bond fragmentations for the MS/MS of the +20 charge state, could be identified by using the 'zoom' and 'ultrazoom' resonance ejection data acquisition scan modes, respectively, indicative of the improved ability to determine product ion charge states under higher resolution conditions. Generally, complementary product ion information was obtained by analysis of each of the different resonance ejection scan mode spectra. A greater number of low abundance product ions were identified from the 'enhanced' scan mode spectra, compared to the higher resolution 'zoom' and 'ultrazoom' scan modes, due to a proportionately greater signal-to-noise ratio for the spectra acquired under lower resolution conditions. However, an overall greater number of product ions could typically be identified from the 'zoom' and 'ultrazoom' spectra, due to the higher resolution associated with these scan modes.

Table 3.2 Summary of the number of amide bond cleavages and percent sequence coverage observed by MS/MS and MS^3 of the WT SaDHNA protein

	Amide bond cleavages observed (Sequence coverage %)		
Resonance Ejection Scan Mode	+18 MS/MS	+20 MS/MS	+20 MS^3
Enhanced	17 (13.4%)	16 (12.6%)	14 (11.0%)
Zoom	30 (23.6%)	30 (23.6 %)	29 (22.8%)
Ultrazoom	36 (28.3%)	15 (11.8%)	47 (37.0%)
	Combined: 64 (50.4%)	Combined: 41 (32.3%)	Combined: 57 (44.9%)
Overall: 85 (66.9%)			

By combining all the data obtained for the +18 charge state, product ions corresponding to fragmentation of 64 of the 127 amide bonds along the protein backbone of the WT SaDHNA protein could be unambiguously identified, corresponding to a sequence coverage of 50.4%. In contrast, a combined sequence coverage of only 32.3% (41 of the 127 amide bonds) was observed for the MS/MS of the +20 charge state. This lower sequence coverage was largely due to the formation of the single dominant product ion at m/z 776.3, corresponding to y_{96}^{14+} in Figure 3.6A, which resulted in 'suppression' of other product ion fragmentation channels and subsequently greater 'losses' of low abundance product ions from the 'ultrazoom' resonance ejection scan mode MS/MS spectrum. Although many of the product ions identified from the +20 charge state were also found in the +18 charge state spectra (Scheme 3.1), several additional product ions

were formed, such that by combining the MS/MS sequence information derived from these two charge states a total of 69 of 127 amide bond cleavages and an overall sequence coverage of 54.3% was obtained for the WT SaDHNA protein. By combining the amide bond cleavage information obtained from the +20 charge state MS/MS and MS^3 spectra, a total of 85 out of the possible 127 amide bond cleavages within the WT SaDHNA protein could be identified (66.9 % sequence coverage).

When all the amide bond cleavages observed from the MS/MS of charge states +8 to +22 were considered along with the MS^3 cleavages from the +20 charge state, the overall sequence coverage obtained was 84.3%, corresponding to 107 of the 127 amide bonds (Scheme 3.2). Three additional cleavages are seen between residues 1-10 when all the charge states are considered, compared to the +18 and +20 charge states alone (compare Scheme 3.1 and 3.2). The amide bond cleavage between residues 5 and 6 was seen for charge states +8 through +17, while the cleavage between residues 6 and 7 was seen for charge states +8 through +16. The cleavage between residues 8 and 9 was seen for the charge states +8 through +10, +12, and +15. Examining another region of the sequence, it can be seen that three additional amide bond cleavages were observed between residues 100-105 when all the charge states were examined. The cleavage between residues 101 and 102 was only seen for the +19 charge state, while the cleavage between resides 102 and 103 was seen for the charge states +12, +15, and +19. Finally, the cleavage between residues 103 and 104 was seen for the +14 charge state only.

Scheme 3.1 Amide bond cleavages observed by top down MS/MS and MS^3 of the +18 and +20 charge states of the WT SaDHNA

Scheme 3.2 Top down MS/MS and MS^3 sequence coverage (+8 to +22 charge states) for the WT. E29A, Y61F, Y61A and E81A show similar fragmentation.

3.5 Characterization of Site-directed Mutagensis Products of the SaDHNA Protein

3.5.1 CID MS/MS and MS^3 of the Y61F, Y61A, E29A, and E81A Site-directed Mutagenesis Products of SaDHNA

Similar to that observed by CID MS/MS of the WT protein, the +18 charge state from the Y61F, Y61A, E29A, and E81A SaDHNA site-directed mutagenesis products showed extensive fragmentation, while the +20 charge state yielded a dominant product ion corresponding to y_{96}^{14+}. The MS^3 fragmentation of the y_{96}^{14+} product from the above SaDHNA mutants was also found to be very similar to that obtained from the WT protein, whereby an extensive series of product ions were formed. Furthermore, the amide bond cleavage sites and the relative abundances of the product ions that were identified from the MS/MS and MS^3 spectra for the mutant proteins were almost identical to those observed in the WT protein, indicating that these mutations did not have any effect on the observed fragmentation behavior. Therefore, by simply identifying the point at which the b- or y-type product ion masses in the SaDHNA mutant proteins diverged from those observed in the WT protein, the site of the modification could be rapidly characterized.

In the MS/MS product ion spectrum obtained from the +18 precursor ion charge state of the Y61F SaDHNA protein (Figure 3.7A), the y_{67}^{9+} ion (m/z 852.0, calculated mass of 7659.0) was found to have an identical m/z value to that observed in the WT protein. In contrast, the y_{68}^{9+} product ion (m/z 868.3, calculated mass of 7805.7) was found to be 16 Da lower than the y_{68}^{9+} product ion from the WT protein (compare the inset of Figure 3.5D to Figure 3.7A). The mass difference of 146.7 Da between the $y_{67}^{9+}$and y_{68}^{9+} ions therefore confirmed that the amino acid at position 61 in the Y61F

SaDHNA protein sequence was a phenylalanine residue, consistent with the expected mutation. As the mass of the y_{96}^{14+} ion determined from MS/MS of the +20 precursor ion charge state (Figure 3.7B) indicated that the mutation was present in this fragment, further confirmation of the specific modification site within the protein was also obtained by MS^3 (Figure 3.7C) via the difference in masses observed between the y_{67}^{9+} and $`b_{60}^{4+}$ product ions. These same ions were seen for the MS/MS and MS^3 product ion spectra from Y61A SaDHNA protein (data not shown), allowing for the confirmation that the mutation in this case was an alanine at position 61.

Figure 3.7

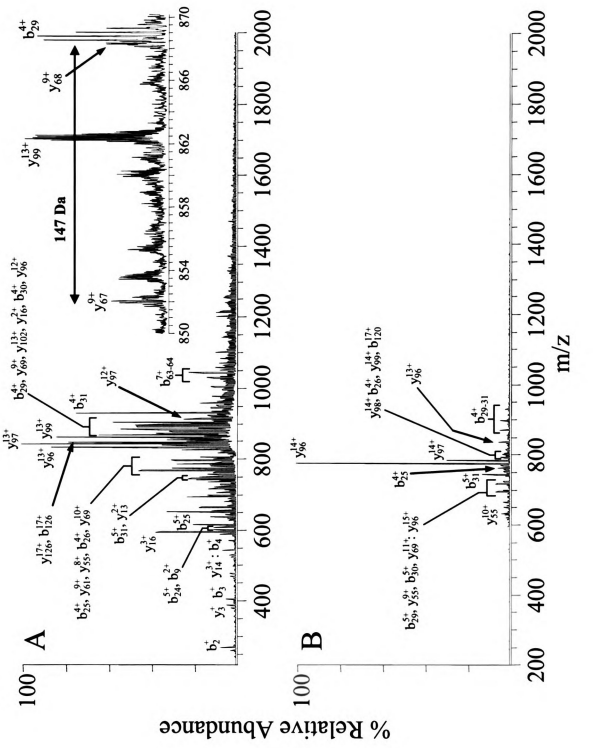
A
B
100
% Relative Abundance
m/z
147 Da
200
400
600
800
1000
1200
1400
1600
1800
2000
850
854
858
862
866
870

Figure 3.7 (continued)

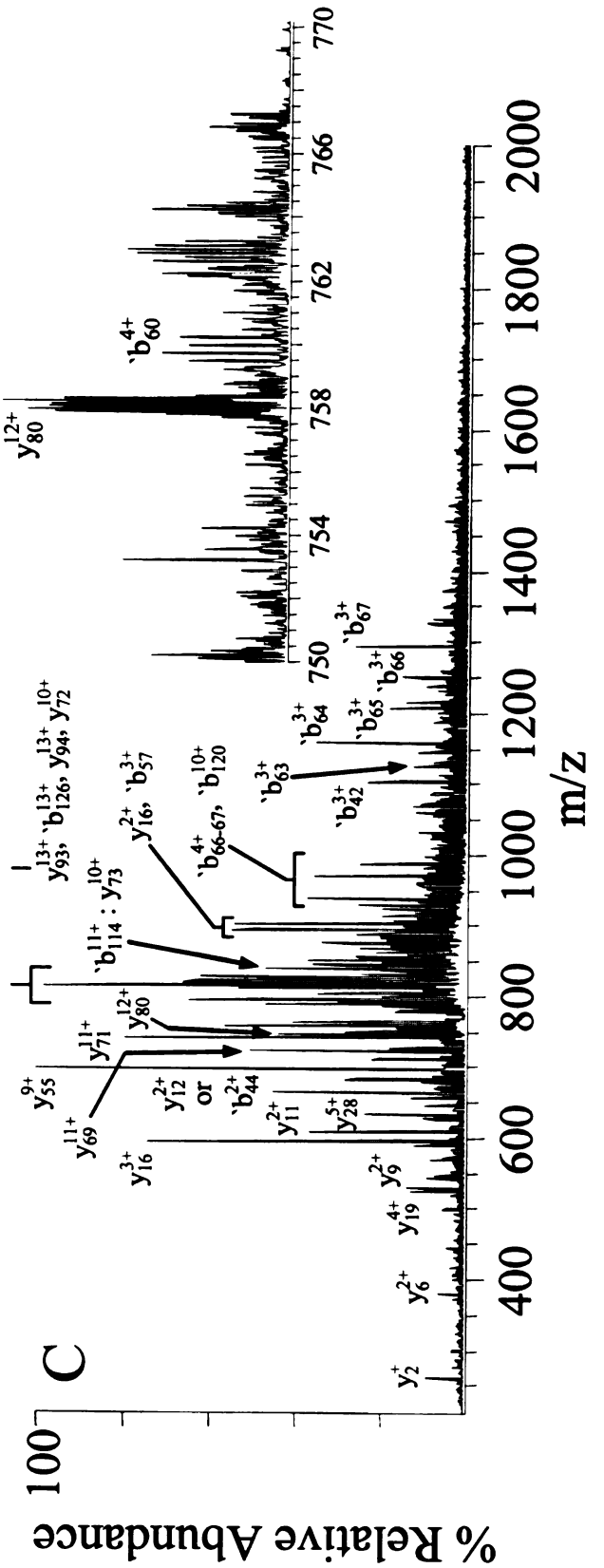

Figure 3.7 (continued) Multistage tandem mass spectrometry characterization of the $[M + 18H]^{18+}$ and $[M + 20H]^{20+}$ precursor ion charge states of the Y61F site-directed mutagenesis product of SaDHNA. (A) 'Zoom' scan mode CID MS/MS product ion spectrum of the $[M + 18H]^{18+}$ ion. The inset to shows the region of m/z from 850 to 870, acquired during an 'ultrazoom' resonance ejection scan, containing the characteristic y_{67}^{9+} and y_{68}^{9+} product ions. (B) 'Zoom' scan mode CID MS/MS product ion spectrum of the $[M + 20H]^{20+}$ ion. (C) 'Zoom' scan mode CID MS^3 product ion spectrum of the y_{96}^{14+} ion obtained by MS/MS from the $[M + 20H]^{20+}$ ion in Figure 3.7B. The inset shows the region of m/z from 750 to 770, acquired during an 'ultrazoom' resonance ejection scan, containing the characteristic `b_{60}^{4+} product ion.

From the MS/MS spectra obtained from the E29A mutant (data not shown), $b_{28}^{5+}$and b_{29}^{5+} product ions, as well as y_{99}^{13+} and y_{100}^{13+} product ions were observed (Scheme 3.1). All of these ions, except for y_{100}, were also found in the MS/MS spectra from the +20 charge state. The b_{28}^{5+} and y_{99}^{13+} ions were both found to have the same masses as that of the WT protein, indicating that the mutation was not located between residues 1 to 28 or residues 30 to 128 of the protein sequence. The b_{29}^{5+} and y_{100}^{13+} ions, however, were shifted in mass compared to their values determined from the WT protein, indicating the location of the mutation at residue 29 of the protein sequence. The difference between the b_{28}^{5+} and b_{29}^{5+} ions for the Y61F protein was 71.3, while the difference between the y_{99}^{13+} and y_{100}^{13+} ions was 71.1 Da, confirming the presence of an alanine residue as the expected mutation. MS^3 was not performed on the dominant y_{96}^{14+} product ion obtained from the +20 charge state of the E29A mutant, as the mass of this ion was found to be identical to that of the WT protein, thereby indicating that the mutation was not located in this region of the protein sequence.

For the E81A mutant (Figure 3.8), although a product ion corresponding to y_{47} was observed in the MS/MS product ion spectra from both the +18 and +20 charge states i.e., fragmentation at the C-terminal side of the expected modification site at residue 81

of the protein sequence, the b_{80} and/or y_{48} product ions that were required to unambiguously locate the site of the modification to this position of the protein sequence were not observed in either spectra. Hence, the modification could only be localized to within residues 77 and 81 of the protein sequence by identification of the y_{52} product ion found in the +18 MS/MS product ion spectra. In contrast, MS^3 of the y_{96}^{14+} product ion from the +20 charge state of the E81A mutant enabled identification of the y_{48} product ion, in addition to the y_{47} product ion mentioned above, thereby allowing localization of the expected glutamic acid modification at residue 81 for this protein. This result is therefore notable in that characterization of the E81A mutant could only be achieved by the use of multiple stages of fragmentation (i.e., MS^3) in the ion trap.

Figure 3.8

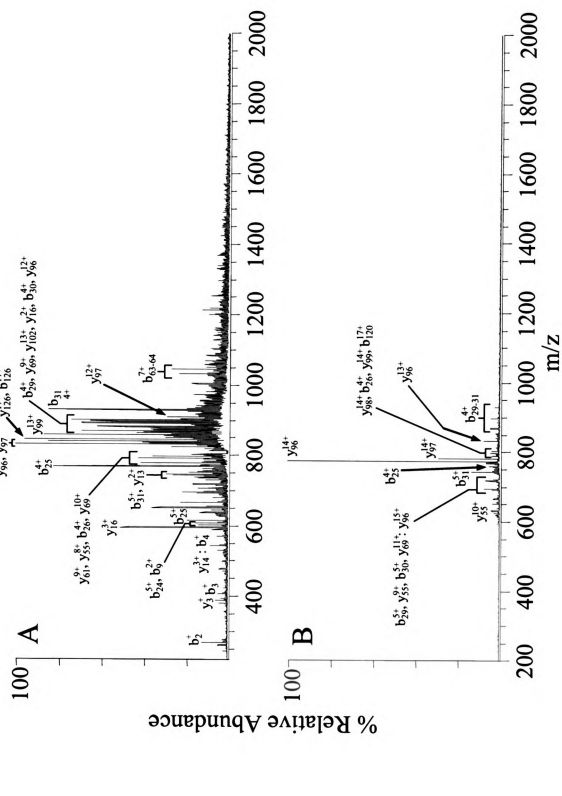
A
B
100
% Relative Abundance
m/z
200
400
600
800
1000
1200
1400
1600
1800
2000

Figure 3.8 (continued)

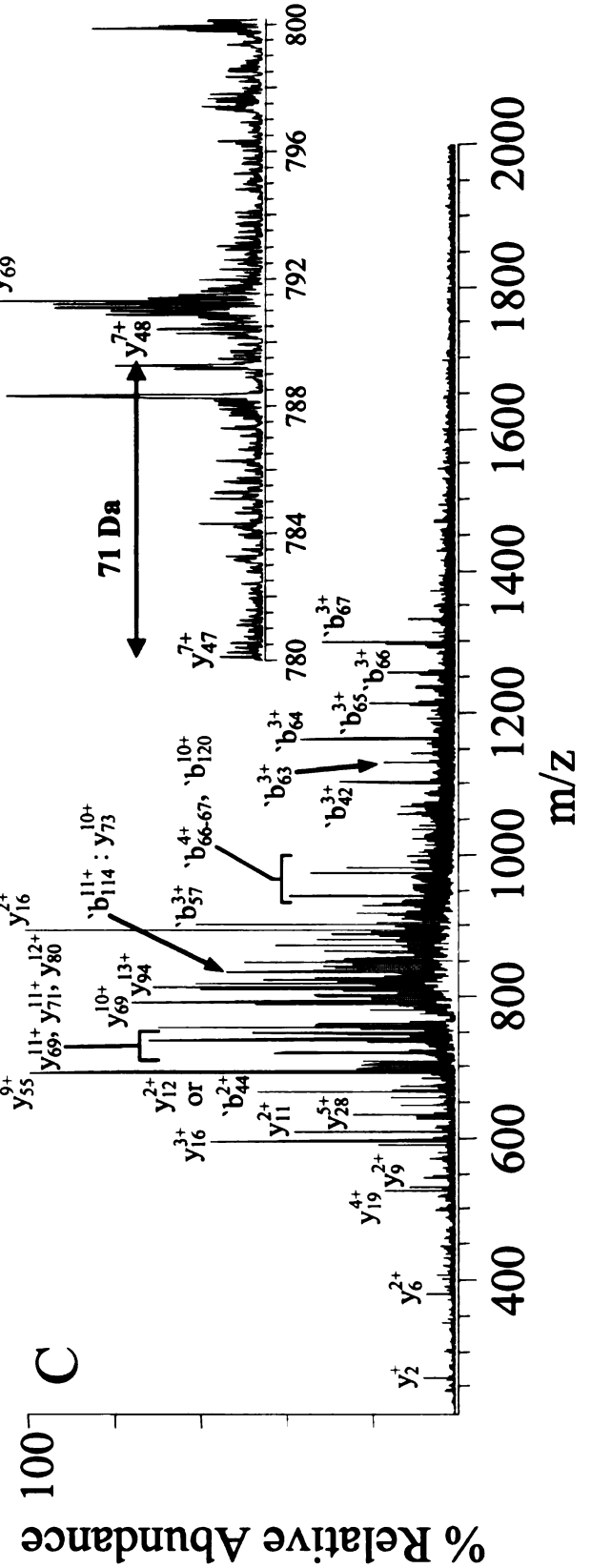

Figure 3.8 (continued) Multistage tandem mass spectrometry characterization of the $[M + 18H]^{18+}$ and $[M + 20H]^{20+}$ precursor ion charge states of the E81A site-directed mutagenesis product of SaDHNA. (A) 'Zoom' scan mode CID MS/MS product ion spectrum of the $[M + 18H]^{18+}$ ion. (B) 'Zoom' scan mode CID MS/MS product ion spectrum of the $[M + 20H]^{20+}$ ion. (C) 'Zoom' scan mode CID MS^3 product ion spectrum of the y_{96}^{14+} ion obtained by MS/MS from the $[M + 20H]^{20+}$ ion in Figure 3.8B. The inset shows the region of m/z from 780 to 800, acquired during an 'ultrazoom' resonance ejection scan, containing the characteristic y_{47}^{7+} and y_{48}^{7+} product ions.

3.5.2 CID MS/MS and MS^3 of the K107A and K107Q Site-directed Mutagenesis Product of SaDHNA

Unlike the Y61F, Y61A, E29A, and E81A site-directed mutagenesis products of the SaDHNA protein described above, dissociation of the K107A (Figure 3.8) and K100Q (data not shown) mutants were observed to result in significantly different product ion spectra than that of the WT protein. The CID MS/MS product ion spectra obtained from the +18 charge state of the K107A mutant protein is shown in Figure 3.8A. It can be seen from this figure that the b_{109}^{14+} product ion, formed by fragmentation at the N-terminal side of the proline residue at position 110 of the protein sequence, was observed as a relatively dominant fragmentation pathway. Interestingly, this ion was not seen as a major product in the +18 charge state MS/MS product ion spectra of the WT protein. The CID MS/MS product ion spectra obtained from the +20 charge state of the K107A mutant protein is shown in Figure 3.8B. Here, although the y_{96}^{14+} product ion was still formed, the y_{96}^{13+} was observed as the most abundant product ion in the spectrum. Furthermore, numerous other product ions were also observed at higher abundance compared to that seen in the WT MS/MS spectrum. MS^3 of the y_{96}^{14+} product ion from Figure 3.8B resulted in the product ion spectrum shown in Figure 3.8C. The appearance of this spectrum is strikingly different to that observed by MS^3 of the y_{96}^{14+} product ion

from the WT protein (Figure 3.6B). Rather than a series of product ions from which extensive sequence information could be derived (as observed by MS^3 of the wild type y_{96}^{14+} product ion), the fragmentation in this case was predominantly directed toward formation of the y_{16}^{3+} and `b_{109}^{10+} product ions, both of which result from cleavage at the N-terminal side of proline residues 113 and 110, respectively, within the protein sequence. MS^3 of the y_{96}^{13+} product ion from Figure 3.8B also gave rise to these product ions (Figure 3.8D), albeit at somewhat lower abundance compared to other product ions that were formed.

Figure 3.9

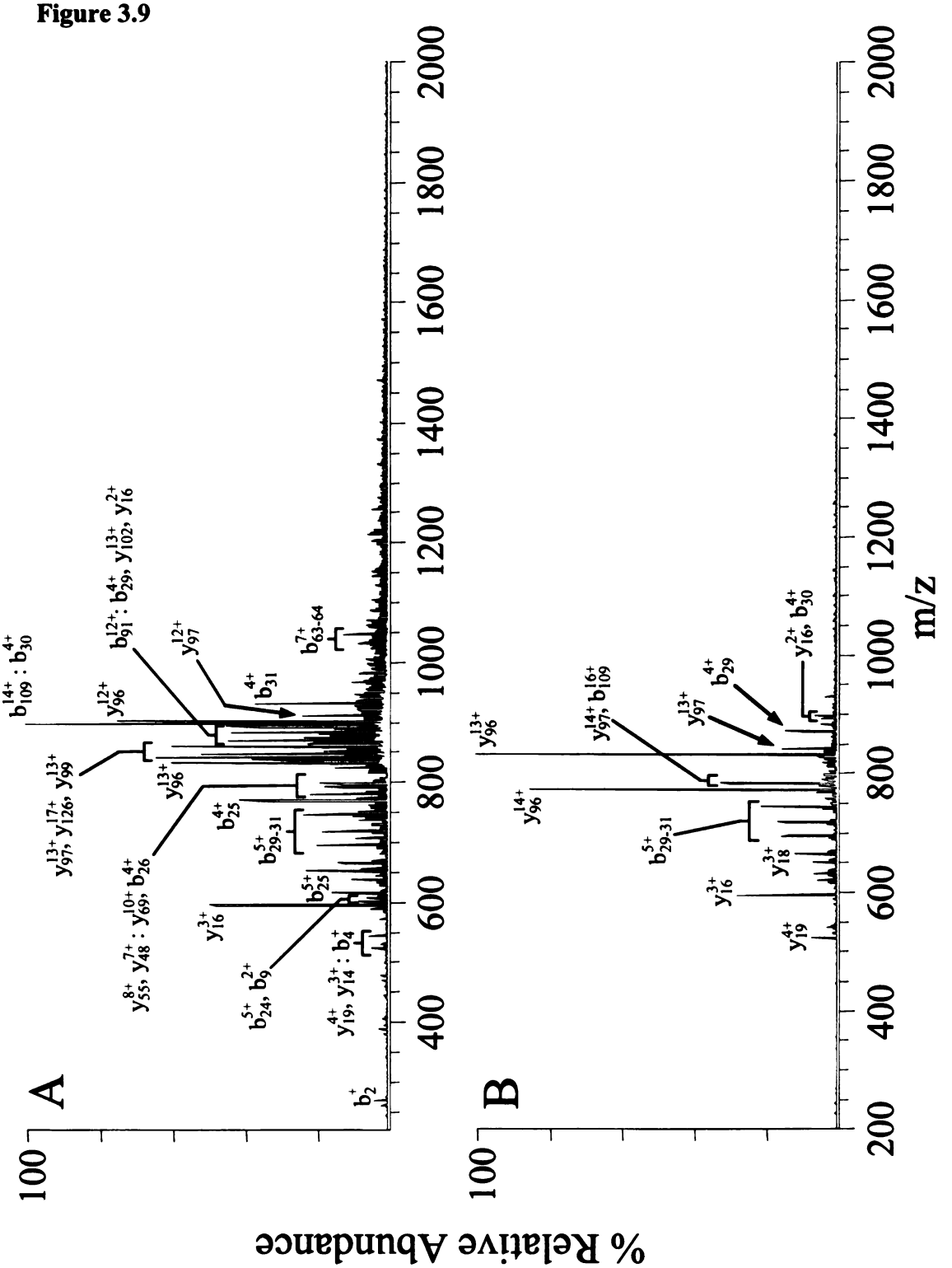
A
B
100
100
% Relative Abundance
m/z
200
400
600
800
1000
1200
1400
1600
1800
2000
$b_{109}^{14+} : b_{30}^{4+}$
y_{96}^{12+}
$b_{91}^{12+} : b_{29}^{4+}, y_{102}^{13+}, y_{16}^{2+}$
y_{97}^{12+}
b_{31}^{4+}
b_{63-64}^{7+}
$y_{97}^{13+}, y_{126}^{17+}, y_{99}^{13+}$
y_{96}^{13+}
b_{25}^{4+}
b_{29-31}^{5+}
$y_{55}^{8+}, y_{48}^{7+} : y_{69}^{10+}, b_{26}^{4+}$
y_{16}^{3+}
b_{25}^{5+}
b_{24}^{5+}, b_9^{2+}
$y_{19}^{4+}, y_{14}^{3+} : b_4^{+}$
b_2^{+}
y_{96}^{13+}
y_{96}^{14+}
$y_{97}^{14+}, b_{109}^{16+}$
b_{29-31}^{5+}
y_{97}^{13+}
b_{29}^{4+}
y_{16}^{3+}
y_{18}^{3+}
y_{16}^{2+}, b_{30}^{4+}
y_{19}^{4+}

Figure 3.9 (continued)

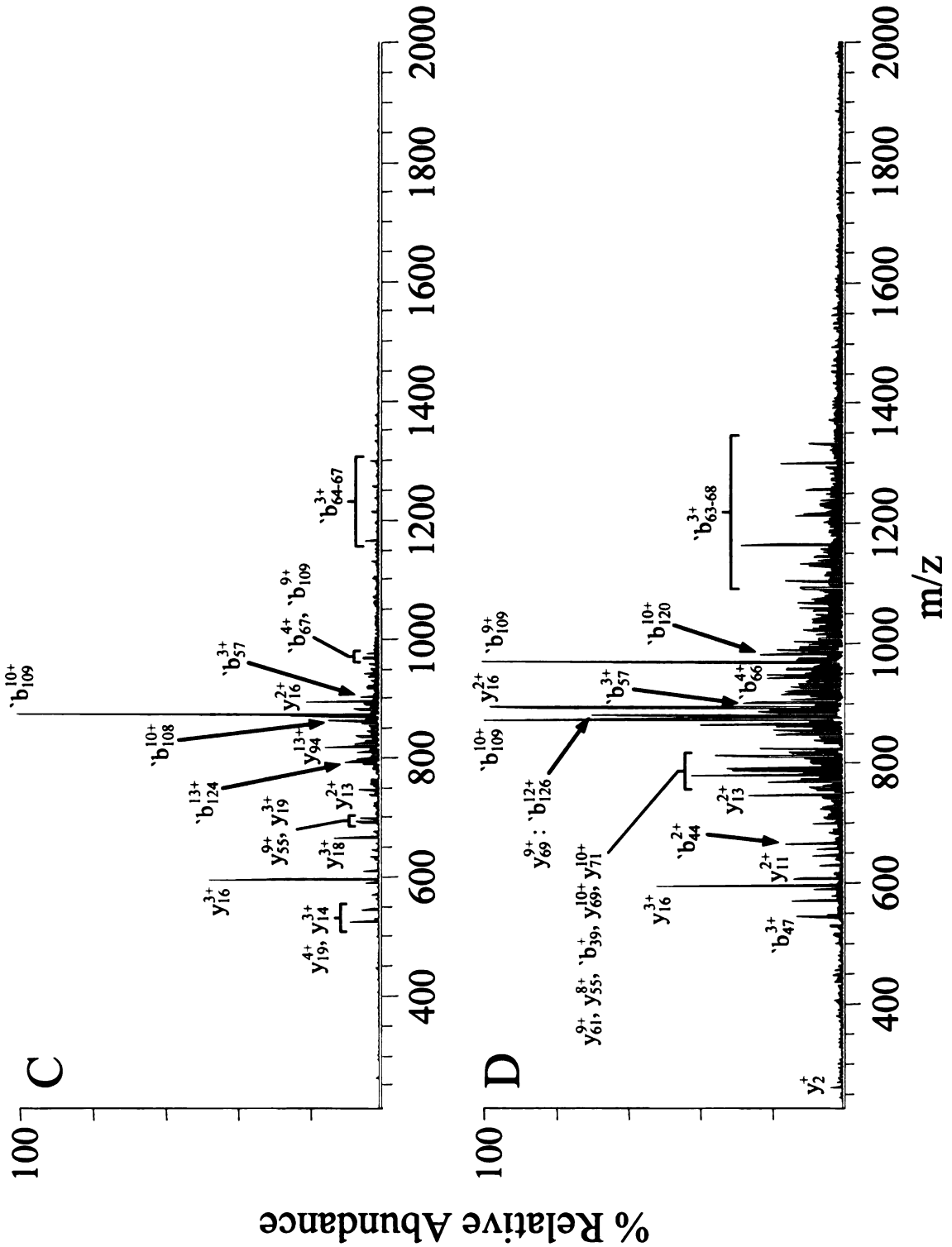

Figure 3.9 (continued) Multistage tandem mass spectrometry characterization of the $[M + 18H]^{18+}$ and $[M + 20H]^{20+}$ precursor ion charge states of the K107A site-directed mutagenesis product of SaDHNA. (A) 'Zoom' scan mode CID MS/MS product ion spectrum of the $[M + 18H]^{18+}$ ion. (B) 'Zoom' scan mode CID MS/MS product ion spectrum of the $[M + 20H]^{20+}$ ion. (C) 'Zoom' scan mode CID MS3 product ion spectrum of the y_{96}^{14+} ion obtained by MS/MS from the $[M + 20H]^{20+}$ ion in Figure 3.8B. (D) 'Zoom' scan mode CID MS^3 product ion spectrum of the y_{96}^{13+} ion obtained by MS/MS from the $[M + 20H]^{20+}$ ion in Figure 3.8B.

Indicative of the greater degree of 'enhanced' fragmentation observed by MS/MS of the +18 and +20 charge states, as well as by MS^3 of the y_{96}^{14+} and y_{96}^{13+} product ions, the identification of only 72 of 127 amide bond cleavage sites within the protein could be obtained for the K107A SaDHNA site-directed mutagenesis product, corresponding to a sequence coverage of 56.7%. Furthermore, due to the more limited sequence coverage observed here compared to the WT SaDHNA protein and previously discussed site-directed mutagenesis products, the modification site in the K107A SaDHNA protein could only be initially localized to within residues 101 to 108 of the protein sequence, by identification of the b_{100}, b_{108} and y_{28} product ions (Scheme 3.3). However, as the 57 Da mass shift observed for the b_{108} and y_{28} product ions in the K107A mutant spectra would result from substitution of only the lysine residues at positions 102 and 107 for alanine, or the arginine residue at position 104 for valine, the site of mutation for the K107A protein may be inferred as being localized to one of these three residues. Interestingly, if dissociation of the K107A mutant had resulted in similar product ion spectra to the WT protein, where the y_{23} and `b_{107} product ions were observed from MS/MS of the +18 charge state and from MS^3 of the y_{96}^{14+} ion from the +20 charge state, respectively, the site of the modification could have been fully characterized.

The K107Q SaDHNA protein shows similar fragmentation and sequence coverage as the K107A protein, however, the mutation of a glutamine for a lysine results in only a 0.04 Da mass shift from the WT. This mass difference is beyond the mass accuracy obtained in these complex spectra. The fact that this protein's fragmentation behavior was almost identically to the K107A protein's behavior is indicative that a mutation had occurred. The mutation itself, however, could not be characterized.

Scheme 3.3 Amide bond cleavages observed by top down MS/MS and MS^3 of the +18 and +20 charge states of the K107A site-directed mutagenesis product of SaDHNA. K107Q shows similar fragmentation.

3.6 **Effect of Charge State on the Fragmentation Behavior of SaDHNA**

Efforts to elucidate the mechanisms and other factors (e.g., secondary or tertiary structure effects) that influence the appearance of product ion spectra derived from the CID MS/MS of multiply charged intact protein ions have not been as extensive as those extended toward understanding the dissociation reactions of protonated peptide ions [55, 59]. However, a consistent picture is starting to emerge regarding the relationship between the charge state and number of basic amino acid residues within a multiply protonated protein ion and its observed fragmentation behavior [37, 39, 43, 56-58]. Cleavage intensity ratio (CIR) calculations were performed for the fragmentation of the WT SaDHNA protein (Figure 3.10). CIR values allow for the quantitative analysis of product ion abundances corresponding to cleavage of each of the amide bonds within a protein ion [55]. The higher a CIR value is the more 'enhanced' the cleavage is. Charge state normalization, however, is important in obtaining accurate CIR values, as the velocity, and thus conversion dynode/electron multiplier detector efficiency, of an ion changes as a function of charge state. Theory predicts that the velocity of an ion increases roughly with the square root of the charge [60]. Thus, in order to normalize for changes in ion detection efficiency due to velocity differences, the intensities of the ions were divided by the square root of their charge prior to CIR calculations.

The WT SaDHNA protein contains a total of 25 basic amino acid residues that, with the exception of the six residue histidine 'tag' at the N-terminus, are relatively evenly distributed throughout the sequence. Thus, the +18 precursor ion of the WT protein corresponds to an 'intermediate' charge state. The y_{96}^{14+} product ion formed from the WT protein contains 16 basic amino acids and is also classified as an 'intermediate'

charge state. The extensive product ion series observed by MS/MS and MS^3 of these ions are therefore generally consistent with previous studies on the charge state dependent fragmentation behavior of intact protein ions [37, 39, 43, 56-58]. In contrast, MS/MS of the +20 charge state of the WT protein, also classified as an 'intermediate' charge state, was observed to give rise to an 'unusual' dominant y_{96}^{14+} product ion by fragmentation between the adjacent $isoleucine_{32}$ and $glycine_{33}$ residues within the protein sequence (Figure 3.10). Enhanced fragmentation at the C-terminal side of isoleucine and leucine residues has been observed previously in the CID MS/MS product spectra of some peptide ions and has been rationalized as being due to local secondary structural effects on the conformation of the gas-phase peptide ions [55]. Additionally, a recent CID MS/MS study on the fragmentation of protonated myoglobin ions in a quadrupole ion trap mass spectrometer has found that the dissociation of 'high' charge states resulted in the formation of an enhanced product ion by fragmentation on the C-terminal side of a leucine residue close to the N-terminal of the protein [56]. Fragmentations of this type, however, are typically observed at lower abundance compared to those resulting from 'enhanced' fragmentations occurring at the C-terminal side of aspartic acid or at the N-terminal side of proline residues. Unfortunately, the effect of many variables that could all play significant roles in influencing the dissociation reactions of intact proteins in the linear ion trap, such as precursor ion charge state, the stability of highly charged b- and y-type product ions, site of protonation, protein sequence, and secondary or tertiary protein structures [61] have not yet been elucidated in sufficient detail to be able to assign a specific cause for the formation of the unusually 'enhanced' y_{96}^{14+} product ion observed here.

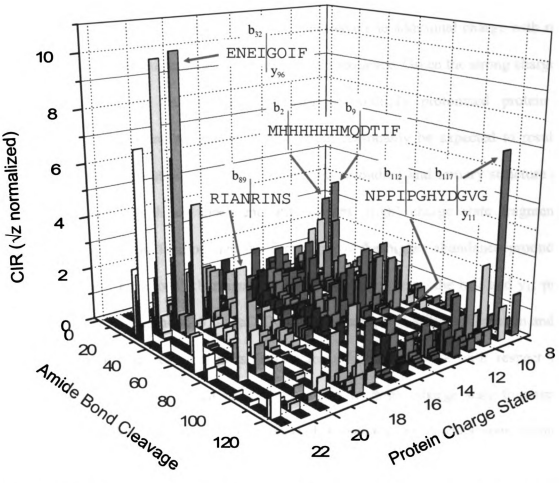

Figure 3.10 Cleavage intensity ratio (CIR) for each possible amide bond cleavage for the WT SaDHNA as a function of charge state. A higher CIR value means a more 'enhanced' cleavage.

It can be seen from the data in Figure 3.9, that the substitution of a single lysine residue resulted in a significant change in the gas-phase fragmentation behavior of the +18 and +20 precursor ions of the K107A SaDHNA proteins and significantly affected the subsequent ability to characterize the site of the modification compared to the WT protein and other sited-directed mutants. Similar to the WT protein, the +18 and +20 precursor ions of the K107A SaDHNA protein, containing a total of 24 basic amino

acids, are both categorized as 'intermediate' charge states. Thus, it may have been expected that these ions would fragment in a similar manner to that of the WT protein. The K107A SaDHNA precursor ions, however, have one additional charge with respect to the number of basic residues within the protein sequence. Given the strong charge state dependence to the fragmentation behavior of multiply protonated protein ions, substitution of a lysine residue to alanine could reasonably be expected to result in a change in the protonation site(s) [61] and/or the secondary and tertiary structure of the K107A mutants, with a subsequent shift toward 'high' charge state fragmentation behaviors. This would rationalize the formation of the higher abundance product ions resulting from 'enhanced' cleavage N-terminal to proline (e.g., the b_{109} and y_{16} product ions in Figure 3.9) in the K107A SaDHNA protein compared to the WT protein and other site-directed mutagenesis products. An increase in charge state with respect to the number of basic residues that resulted in a shift to 'high' charge state fragmentation behaviors would also explain the increased abundance of product ions formed by fragmentation N-terminal to proline in the MS^3 spectra from the y_{96}^{14+} and y_{96}^{13+} product ions (Figures 3.9C and D, respectively). Finally, the increased abundance of the y_{96}^{13+} product ion from MS/MS of the +20 charge state of the K107A SaDHNA mutants (Figure 3.9B) may be readily explained in terms of the decreased propensity for the y_{96} product ion to retain all 14 charges when one basic residue has been removed.

3.7 Conclusions

The gas-phase fragmentation reactions of a series of site-directed mutagenesis products of *Staphylococcus aureus* dihydroneopterin aldolase have been examined by

multistage tandem mass spectrometry (MS/MS and MS^3) in a linear quadrupole ion trap in order to explore the utility of this instrumentation for routine 'top down' recombinant protein characterization. Following a rapid low resolution survey of the fragmentation behavior of the precursor ions from the wild type (WT) protein, selected charge states were subjected to detailed structural characterization by using high resolution 'zoom' and 'ultrazoom' resonance ejection MS/MS product ion scans. Dissociation of the $[M + 18H]^{18+}$ charge state yielded a range of product ions from which extensive sequence information could be derived. In contrast, dissociation of the $[M + 20H]^{20+}$ charge state resulted in a single dominant y_{96} product ion formed by fragmentation between adjacent Ile/Gly residues, with only limited sequence coverage. Further extensive sequence information was readily obtained, however, by MS^3 dissociation of this initial product.

MS/MS and MS^3 of four of the six site-directed mutagenesis products (E29A), (Y61F), (Y61A), and (E81A) were found to yield essentially identical product ion spectra to the WT protein, indicating that these modifications had no significant influence on the fragmentation behavior. The specific site of modification could be unambiguously determined in each case by characterization of product ions resulting from fragmentation of amide bonds on either side of the mutation site. In contrast, MS/MS and MS^3 of the K107A and K107Q mutants led to significantly different product ion spectra dominated by cleavages occurring N-terminal to proline, which restricted the ability to localize the modification site.

Although the factors that govern the fragmentation reactions of multiply protonated intact protein ions under low energy CID conditions have not yet been fully elucidated, the results obtained here indicate that multistage tandem mass spectrometry

coupled with high resolution resonance ejection scans in the linear quadrupole ion trap may be employed for the routine 'top down' characterization of recombinant proteins of modest (<20 kDa) size. The results of this study, combined with future studies, will aid the long term goal of developing improved mass spectrometry based approaches and database search and scoring algorithms for use in routine, automated protein identification and characterization strategies.

CHAPTER FOUR

Characterization of the Substrate Reactivity of *Staphylococcus aureus* Dihydroneopterin Aldolase and its Y61F Site-directed Mutagenesis Product Using a Linear Quadrupole Ion Trap*

4.1 Introduction

The ability for microbes to rapidly develop resistance against current antibiotic drugs requires renewed effort in the development of new antimicrobial agents. Among the most promising strategies for the development of new antibacterial therapeutics is the targeting of proteins that are essential for bacterial growth but are lacking in mammalian counterparts. Dihydroneopterin aldolase (DHNA) is one such protein [62]. It catalyzes the conversion of 7, 8-dihydroneopterin (DHNP) (**Structure 1**) to 6-hydroxymethyl-7, 8-dihydroneopterin (HP) (**Structure 2**) in the folate biosynthetic pathway of most microorganisms. As mammalian systems have an active transport system for deriving essential folates from their diet, and therefore lack this pathway, the folate biosynthetic pathway is an attractive target for the development of antimicrobial agents [63]. *Staphylococcus aureus* (*S. aureus*) is a bacterium that has become resistant to many commonly used antibiotics and it therefore an attractive target organism for the development of these agents.

---

* The results described in this Chapter have been published in: Yan, H; Scherperel, G.; Roberts, K.D.; Jones, A.D.; Reid, G.E. and Yan, H. A point mutation coverts dihydroneopterin aldolase to a cofactor-independent oxygenase. *J. Am. Chem. Soc.* **2006,** 128, 13216-13223.

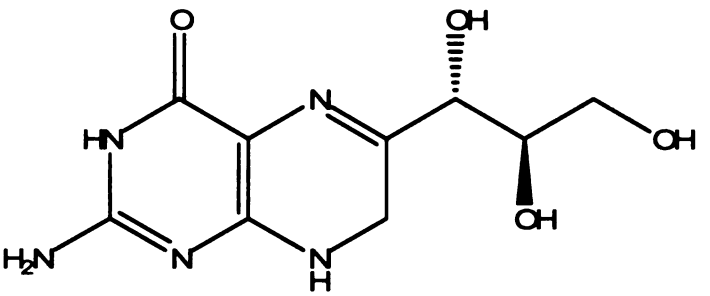

Structure 1: DHNP

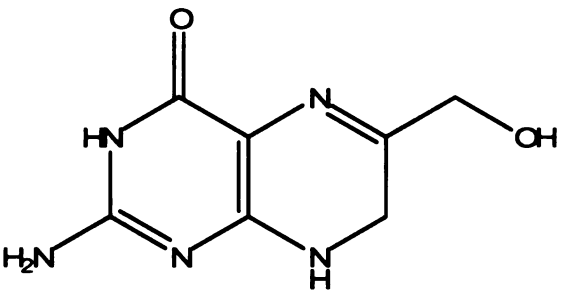

Structure 2: HP

The crystal structure of the octomeric enzyme-substrate complex of *Staphylococcus aureus* dihydroneopterin aldolase (SaDHNA) with the product HP **(2)** has previously been determined by high resolution X-ray crystal structure analyses [64]. It is understood that the enzymatic reaction takes place in the confines of the eight active sites of the octomeric enzyme. Figure 4.1 shows the specific active site residues and their interaction with the product, HP **(2)**, determined from the crystal structure. Each active site contains an important water molecule along with four conserved residues, E29, E81, and K107 from one subunit and Y61 from an adjacent subunit. The pterin ring of HP **(2)** is stacked with the phenol ring of Y61. The hydroxyl group of the phenol ring of Y61 forms a hydrogen bond with the hydroxyl group of HP **(2)** as well as with the amino

group of K107. The carboxyl group of E29 forms a hydrogen bond with the hydroxyl group of HP **(2)** and with the amino group of K107. The carboxyl group of E81 forms two hydrogen bonds with HP **(2)**. In addition to the hydrogen bonds with E29 and Y61, K107 also forms a hydrogen bond with a water molecule, which is in turn hydrogen bonded to N5 of HP **(2)**, which is notable because there is no residue in SaDHNA that can form a hydrogen bond directly with N5 of HP **(2)**.

While the crystal structures of SaDHNA have provided a three-dimensional view of the active sites of the enzymes, the functional roles of the active site residues are yet to be established. Thus, site-directed mutagenesis was used to remove the functional groups at the active sites within the enzyme. Changes in the binding and catalytic properties of the enzymes were then measured to determine the functional roles of these residues [54]. Of particular interest was a mutation involving the active site tyrosine residue, which was found to confer unique new chemistry to the enzyme, later identified as an oxygenase.

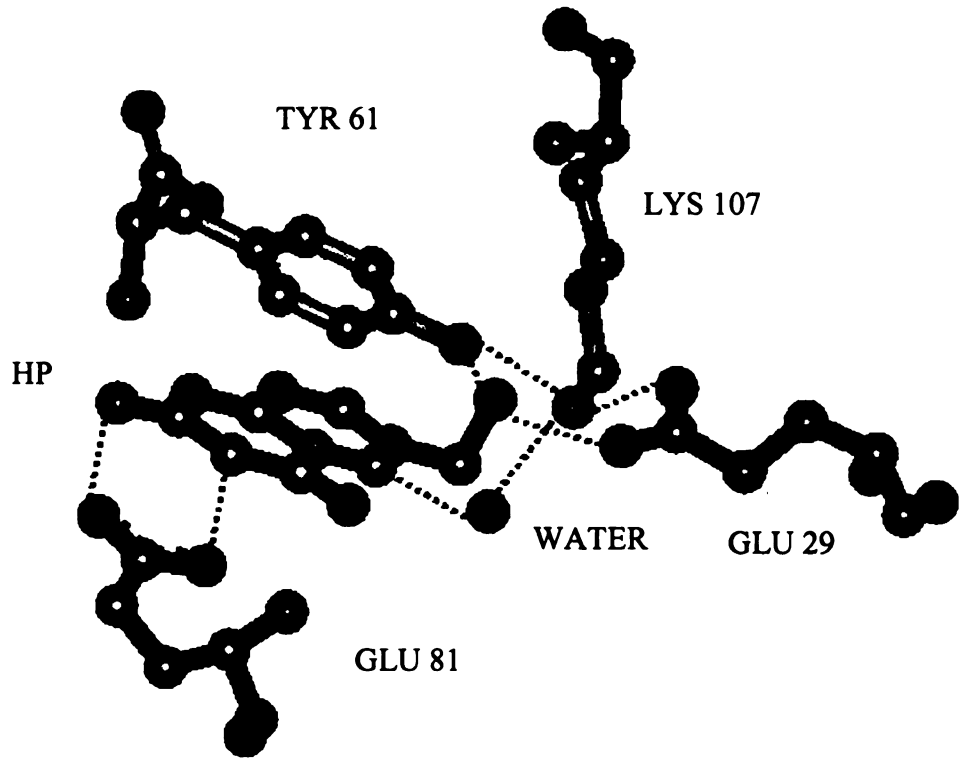

Figure 4.1 The potentially important residues around the product HP **(2)** at the active site of SaDHNA. The residues shown are E22, Y54, E74, and K100. A water molecule is found close to N5 of HP **(2)**. The dotted lines represent hydrogen bonds.

4.2 Initial Experiments

Initial biochemical analysis revealed that there was a dramatic decrease in the fluorescence intensity of the reaction mixture from the Y61F site-directed mutagenesis product of SaDHNA, which was not observed for the reaction mixture for the wild-type (WT) SaDHNA [65]. This was indicative that the mutant enzyme-catalyzed reaction generated different products that that of the WT enzyme-catalyzed reaction. In order to confirm this, nuclear magnetic resonance (NMR) was utilized [65]. This showed that the major product of the mutant-catalyzed reaction was a compound with a proton peak at 4.12 ppm, while the major product for the WT reaction was a compound with a proton

peak at 4.18 ppm. Mass spectrometry was then used to identity these products and to provide further insight into the changes in enzyme activity conferred by the mutations.

4.3 Mass Spectrometry Identification of Products

As a first step, an ESI mass spectra was acquired from two separate 10 minute reactions of DHNP **(1)** with the WT SaDHNA and with the Y61F SaDHNA site-directed mutatgenesis product enzyme, respectively (Figure 4.2). A cursory examination of this figure confirmed that the primary product formed by reaction of the substrate, DHNP **(1)**, with the WT SaDHNA protein was different than the primary product observed by reaction of DHNP **(1)** with Y61F SaDHNA. The mass spectrum of the reaction involving the WT protein (Figure 4.2A) showed the formation of the expected HP **(2)** product ion at m/z 196, while the spectrum of the reaction involving the mutant Y61F protein (Figure 4.2B) showed the formation of a novel product ion at m/z 182.

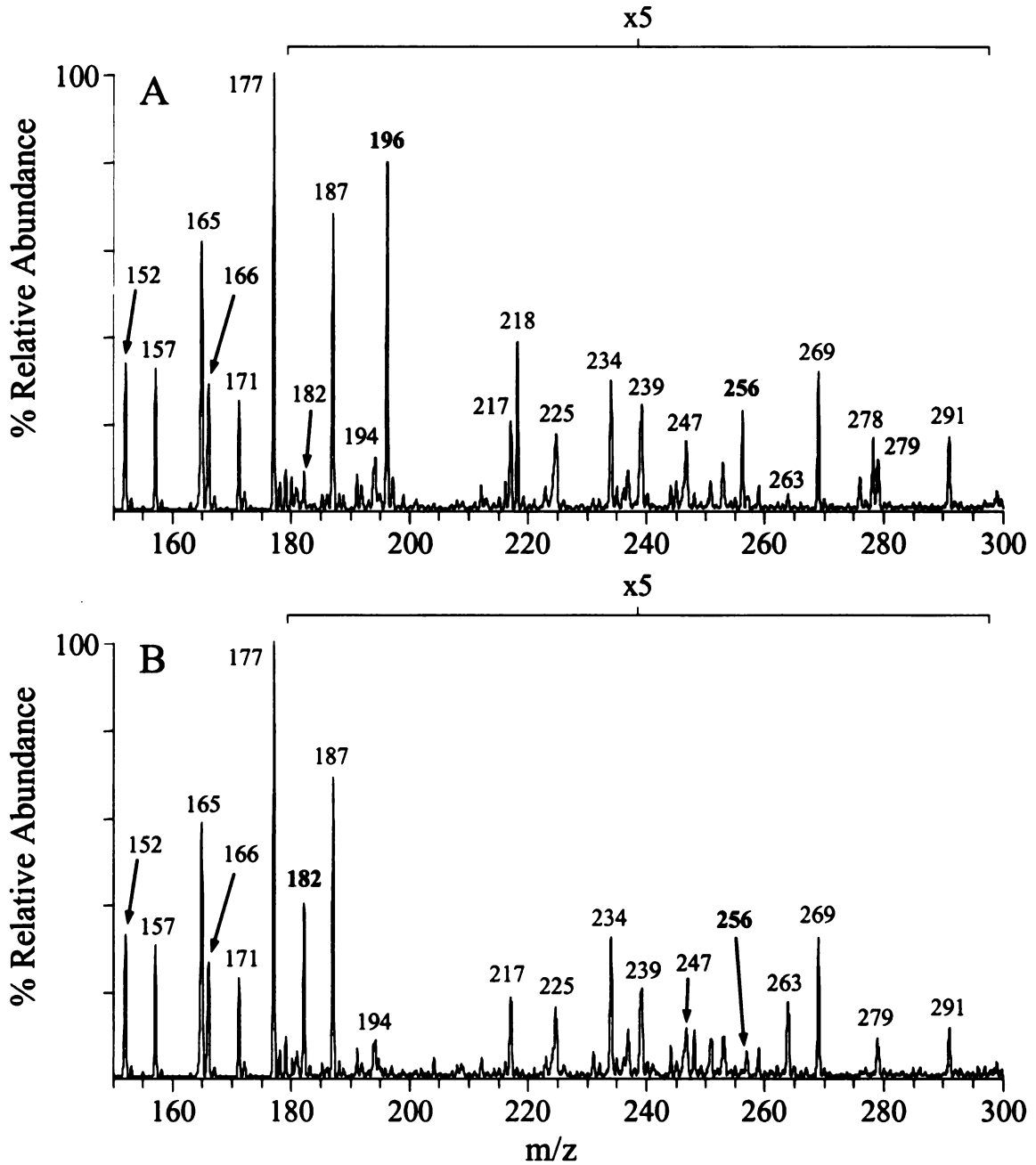

Figure 4.2 ESI mass spectra from a 10 minute reaction of DHNP **(1)** with (A) the WT SaDHNA protein and (B) the Y61F SaDHNA. The unreacted substrate, DHNP **(1)**, is at m/z 256 in both spectra. The region from m/z 180-300 has been magnified (x5) for clarity.

Tandem mass spectrometry was used to confirm that the ion at m/z 256 in Figure 4.2 was that from the substrate DHNP **(1)** (Figure 4.3). MS/MS and MS^3 spectra were obtained and compared to the MS/MS and MS^3 spectra of a standard DHNP **(1)** solution. An examination of Figure 4.3 indicated that the major ions observed by CID MS/MS of the ion at m/z 256 obtained from the WT reaction after 10 minutes (from Figure 4.2A) were identical to the major product ions seen in the MS/MS product ion spectrum obtained from the standard (compare Figures 4.3A and B). The most abundant product ion in Figures 4.3A and B at m/z 238 was most likely due to the loss of water from the precursor ion. MS^3 was then performed on the m/z 238 product ion (Figures 4.3C and D) and the experimental and standard spectra were essentially identical. The most abundant product ion at m/z 220 was most likely due to the loss of H_2O. Thus, the MS/MS and MS^3 spectra provide strong evidence that the ion seen at m/z 256 from the reaction of DHNP **(1)** with the SaDHNA protein was the unreacted substrate DHNP **(1)**.

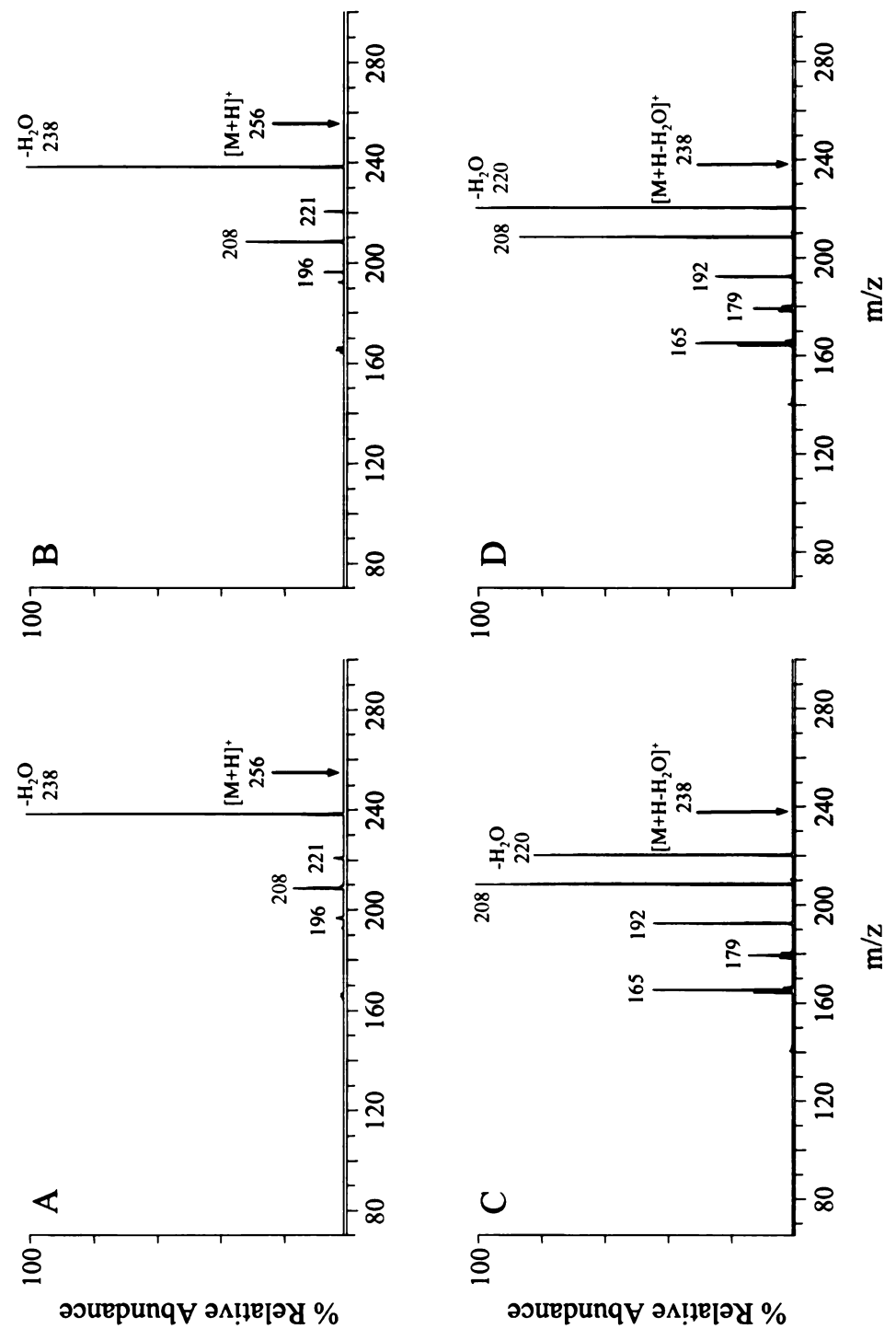

Figure 4.3 Multistage tandem mass spectrometry identification of the substrate DHNP **(1)**. (A) CID MS/MS product ion spectrum of the ion at m/z 256 obtained from Figure 4.2A. (B) CID MS/MS product ion spectrum of the m/z 256 precursor ion obtained from a standard solution of DHNP **(1)**. (C) CID MS^3 product ion spectrum of the ion at m/z 238 in Figure 4.3A. (D) CID MS^3 product ion spectrum of the ion at m/z 238 in Figure 4.3B.

In order to confirm the identity of the m/z 196 ion in Figure 4.2A, MS/MS and MS^3 spectra were obtained and compared to the MS/MS and MS^3 spectra of the proposed reaction product, HP **(2)** (Figure 4.4). An examination of Figure 4.4 indicated that the major ions observed by CID MS/MS of the ion at m/z 196 obtained from the WT reaction after 10 minutes (from Figure 4.2A) were identical to the major product ions seen in the MS/MS product ion spectrum obtained from the standard (compare Figures 4.4A and B). The most abundant product ion in Figures 4.4A and B at m/z 178 was most likely due to the loss of water from the precursor ion. To obtain further confirmation of the expected product ion structure, MS^3 was then performed on the m/z 178 product ion (Figures 4.4C and D). As expected, the experimental and standard MS^3 spectra were essentially identical. The most abundant product ions at m/z 161 and 150 were most likely due to the loss of NH_3 and CO, respectively. Based on an MS^4 experiment (data not shown), the MS^3 product ion seen at m/z 179 was formed via an ion-molecule reaction between the ion at m/z 161 and a water molecule. Taken together, the MS/MS and MS^3 spectra provide strong evidence that the product seen at m/z 196 from the reaction of DHNP **(1)** with the WT SaDHNA protein was HP **(2)**.

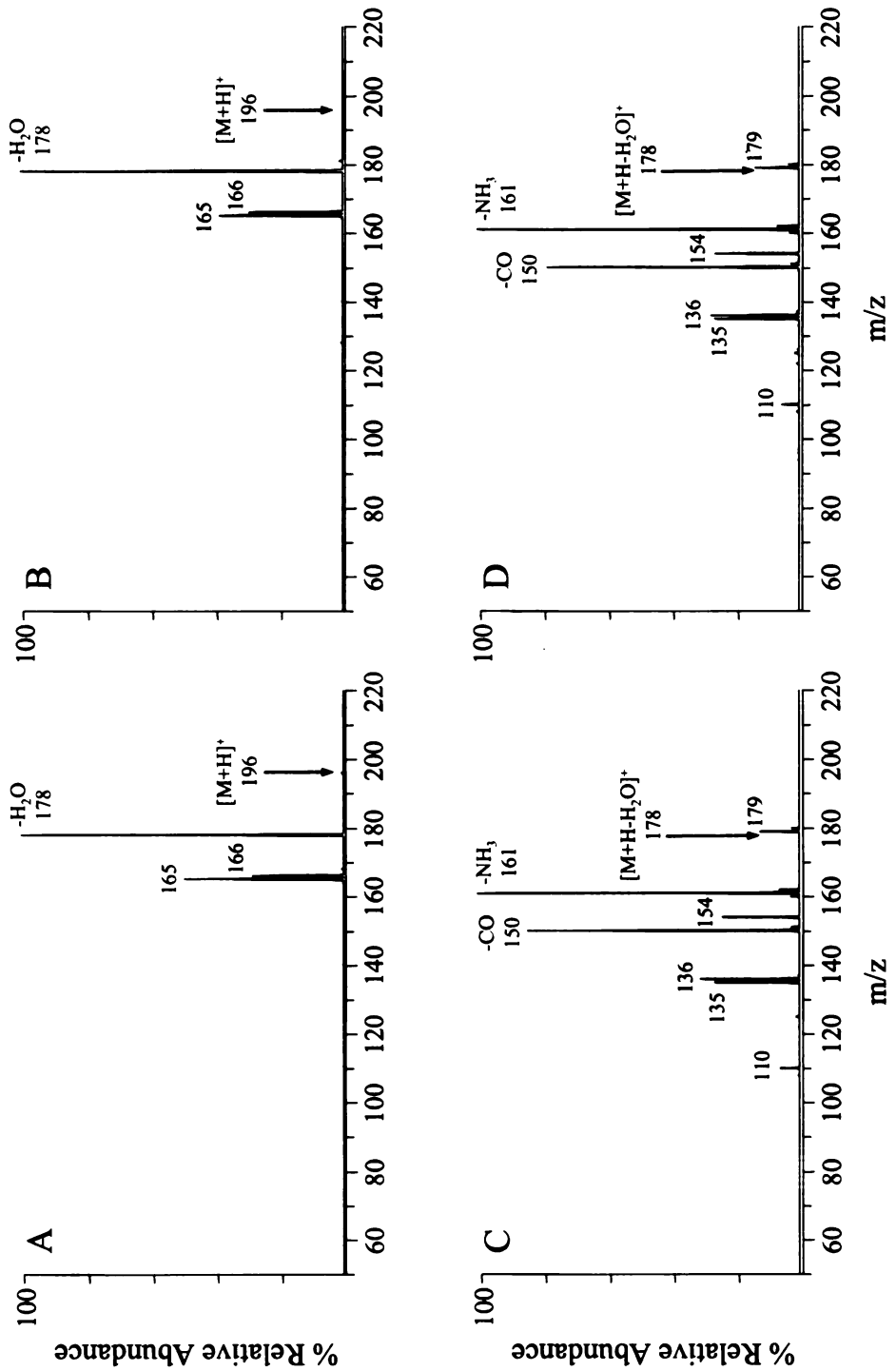

Figure 4.4 Multistage tandem mass spectrometry identification of the m/z 196 product from the reaction of DHNP **(1)** with the WT SaDHNA protein. (A) CID MS/MS product ion spectrum of the ion at m/z 196 obtained from Figure 4.2A. (B) CID MS/MS product ion spectrum of the m/z 196 precursor ion obtained from a standard solution of HP **(2)**. (C) CID MS^3 product ion spectrum of the ion at m/z 178 in Figure 4.4A. (D) CID MS^3 product ion spectrum of the ion at m/z 178 in Figure 4.4B.

This same type of analysis was also performed in order to determine the identity of the m/z 182 ion in Figure 4.2B. MS/MS and MS^3 spectra were obtained for the ion at m/z 182 obtained from the Y61F mutant reaction after 10 minutes (from Figure 4.2B). Based on the fragmentation behavior seen for this ion and the key loss of CO (28 Da), it was proposed that the reaction product corresponded to 7,8-dihydroxanthopterin (DHXP) (**Structure 3**). In order to confirm this, the experimental MS/MS and MS^3 spectra (Figure 4.5A and C) were compared to MS/MS and MS^3 spectra of a standard solution of DHXP (Figure 4.5B and D). The major ion observed by CID MS/MS of the ion at m/z 182 obtained from the Y61F mutant reaction after 10 minutes was identical to the major ion seen in the MS/MS product ion spectrum obtained from the standard (compare Figures 4.5A and B). The product ions at m/z 154 in Figures 4.5A and B were most likely due to the loss of CO from the precursor ion. MS^3 was then performed on the m/z 154 ion (Figures 4.5C and D). Again, the experimental and standard spectra were essentially the same. The major MS^3 product ion seen, at m/z 126, corresponded to the loss of CO, while the second most intense ion, seen at m/z 137, corresponded to the loss of NH_3. As was the case for the previous analysis of the WT reaction, these spectra together provide strong evidence that the product seen at m/z 182 from the reaction of DHNP (**1**) with the Y61F site-directed mutagenesis product of SaDHNA was DHXP (**3**).

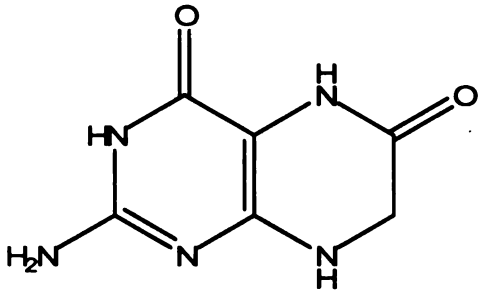

Structure 3: DHXP

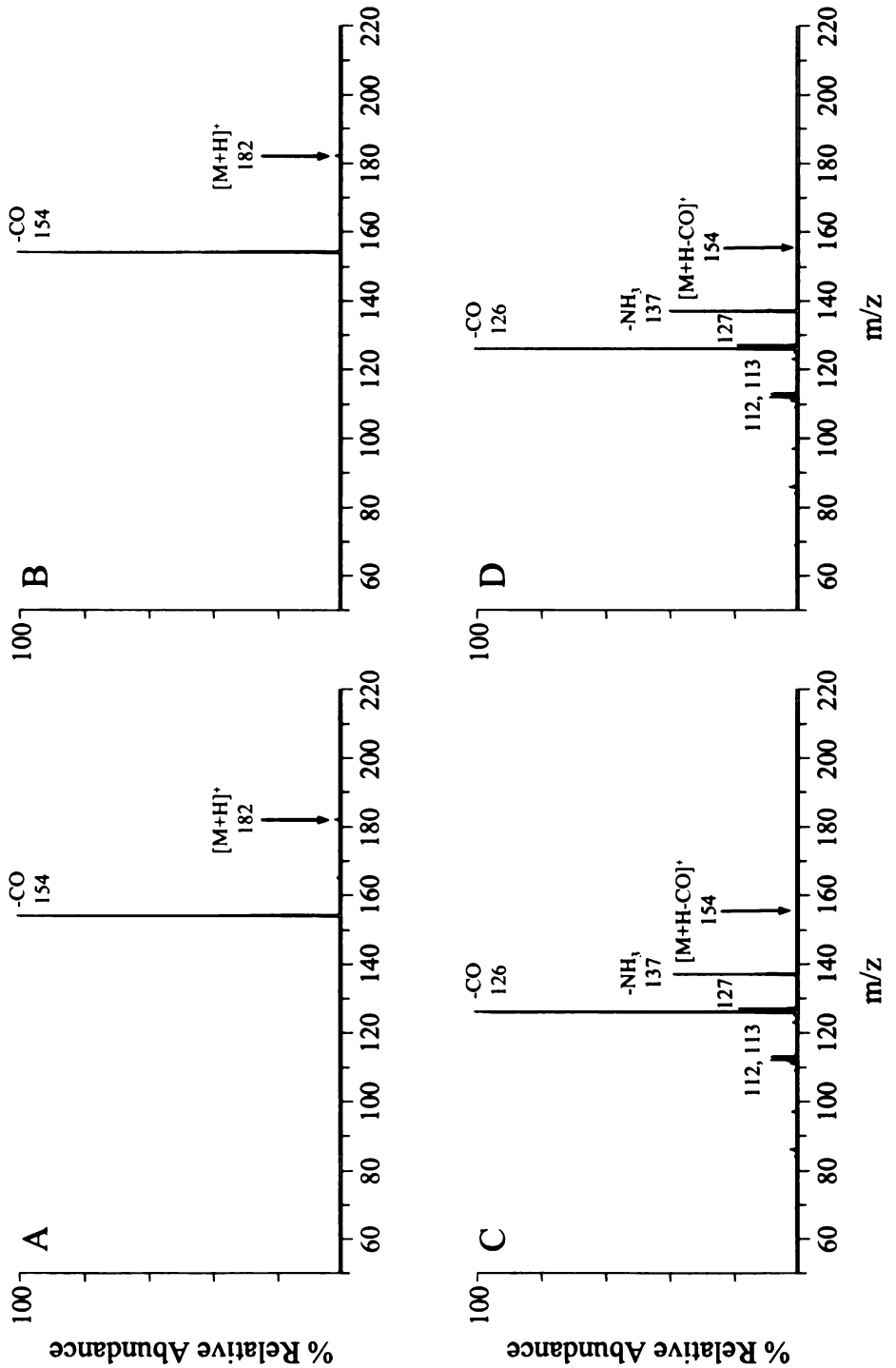

Figure 4.5 Multistage tandem mass spectrometry identification of the m/z 182 product from the reaction of DHNP **(1)** with the Y61F SaDHNA. (A) CID MS/MS product ion spectrum of the ion at m/z 182 obtained from Figure 4.2B. (B) CID MS/MS product ion spectrum of the m/z 182 precursor ion obtained from a standard solution of DHXP **(3)**. (C) CID MS^3 product ion spectrum of the ion at m/z 154 in Figure 4.5A. (D) CID MS^3 product ion spectrum of the ion at m/z 154 in Figure 4.5B.

Once the major products from both reactions had been identified, an MS time course experiment of the DHNP **(1)** reaction was performed, as shown in Figure 4.6. At 0 minutes into the reaction of DHNP **(1)** with the WT SaDHNA protein (Figure 4.6A), the DHNP **(1)** substrate ion at m/z 256 was more abundant than the ion at m/z 196. The same is true for the reaction of DHNP **(1)** with the Y61F mutant protein (Figure 4.6B), where at 0 minutes the abundance of the DHNP **(1)** ion was significantly larger than that for the ion at m/z 182. However, after 10 minutes, the ions at m/z 196 and m/z 182, for the WT and mutant proteins reactions respectively, increased as the DHNP **(1)** peaks decreased. Thus, as the abundance of DHNP **(1)** (m/z 256) decreased over time as a result of being consumed by the reaction, Figure 4.6A showed an increase in the abundance of m/z 196, while Figure 4.6B showed an increase in the abundance of m/z 182. This supports the data shown in Figure 4.2, i.e., that the ions at m/z 196 and m/z 182 are the products of the reaction of DHNP **(1)** with the WT SaDHNA protein and the Y61F SaDHNA mutant protein, respectively. Furthermore, there was no accumulation of HP **(2)** in the mutant-catalyzed reaction, suggesting that DHXP **(3)** was not derived from HP **(2)**, unless the conversion of HP **(2)** to DHXP **(3)** was much faster than the formation of HP **(2)**.

In order to confirm that the ion seen at m/z 182 is a direct product of the reaction of DHNP **(1)** with the Y61F mutant SaDHNA protein and not from the rapid conversion of HP **(2)** (m/z 196) to DHXP **(3)** (m/z 182), HP **(2)** was added to a solution of the Y61F SaDHNA. If DHXP **(3)** was due to a conversion then, over time, these spectra should show a decrease in the intensity of m/z 196 and an increase in the intensity of m/z 182. There was not, however, any production of the ion at m/z 182 seen in these spectra (not

shown), indicating that this ion was indeed formed directly from the reaction of DHNP **(1)** with the mutant protein and not due to a conversion. This data set also confirmed that none of the ions seen were the result of HP **(2)** reacting with the protein because none of the ion abundances changed significantly, indicating that no reaction was taking place. The same experiment was performed with the WT SaDHNA protein whose spectra (data not shown) again showed no reaction between HP **(2)** and the WT protein. This confirmed that both the ion at m/z 182 and the ion at m/z 196 were direct products of the reactions of DHNP **(1)** with the Y61F site-directed mutagenesis product of SaDHNA and the WT SaDHNA, respectively.

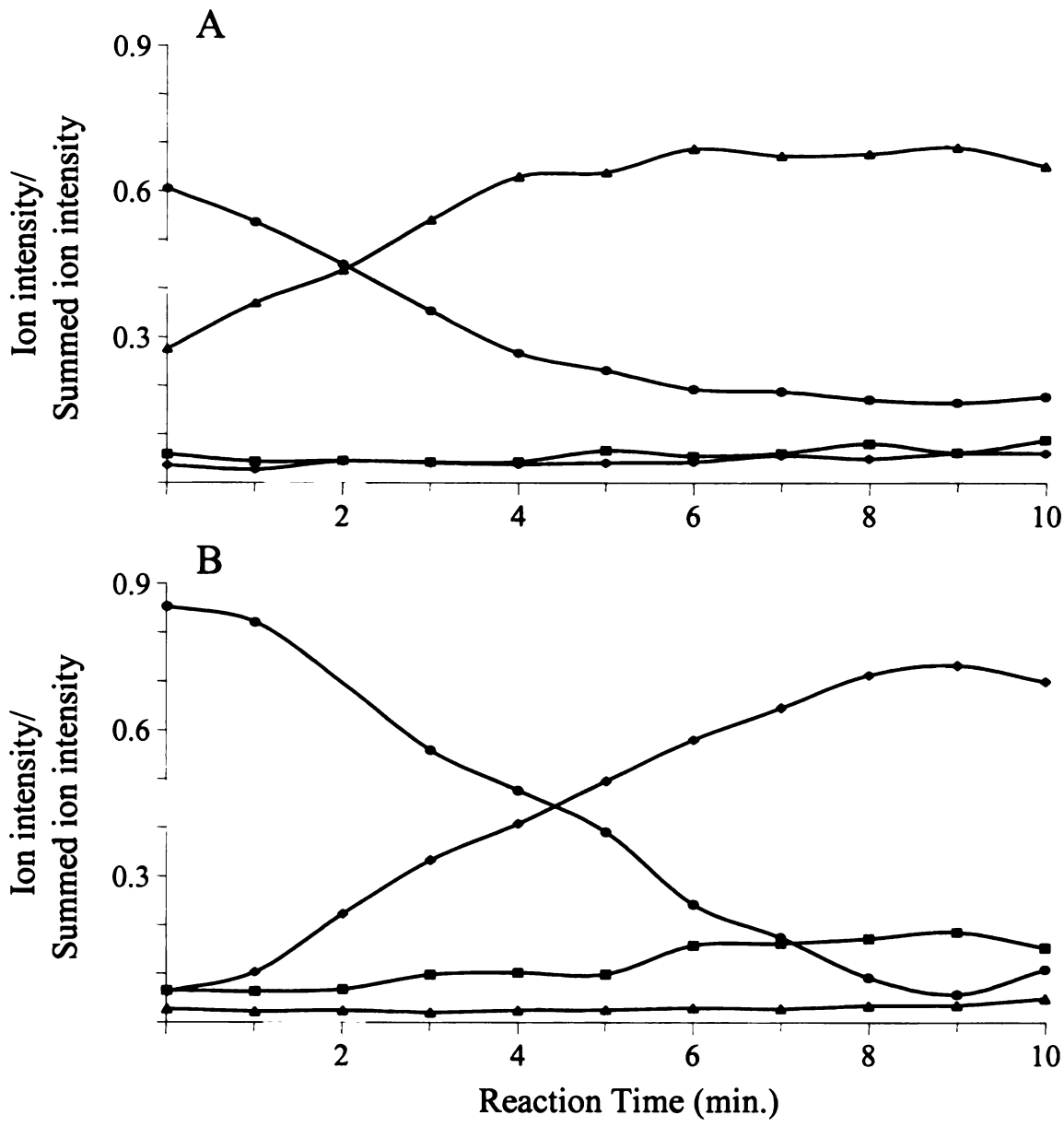

Figure 4.6 MS time course experiment for the reaction of DHNP **(1)** with (A) the WT SaDHNA protein and (B) the Y61F SaDHNA. (● = m/z 256, ■ = m/z 194, ▲ = m/z 196, ♦ = m/z 182)

In addition to the ions at m/z 182, 196, and 256, Figure 4.6 also tracked the change in the abundance of the ion at m/z 194 over time because it is likely that it was 6-hydroxymethylpterin (HPO) and its tautomer 6-formyl-7,8-dihydropterin (FDHP) (**Structure 4**). In Figure 4.6A, the abundances of the ions at m/z 182 (product of mutant catalyzed reaction) and m/z 194 stayed relatively constant throughout the time course of the experiment indicating that they are neither produced nor consumed by the reaction of DHNP **(1)** with the WT SaDHNA protein. In Figure 4.6B, however, while the abundance of the ion at m/z 196 (product of WT reaction) did not alter significantly over time as would be expected, there was a slight increase in the abundance of the ion at m/z 194. By collecting MS/MS and MS^3 spectra from standard solutions of both HPO and the tautomer FDHP **(4)**, the identity of the ion at m/z 194 in Figure 4.6B could be achieved. CID MS/MS of the ion at m/z 194 from the 10 minute reaction of DHNP **(1)** with the Y61F SaDHNA mutant protein (from Figure 4.2 B) yielded two product ions, one at m/z 176 and the other at m/z 165. (Figure 4.7A) MS/MS of the HPO standard, on the other hand, yielded only one product ion at m/z 176, while MS/MS of the FDHP **(4)** standard yielded one product ion at m/z 165 (Figures 4.7B and C, respectively). The MS^3 spectrum of the ion at m/z 176 from the experimental reaction matched the MS^3 spectrum of the ion at m/z 176 from the HPO standard (Figures 4.7D and E, respectively). The MS^3 spectrum of the ion at m/z 165 from the experimental reaction matched the MS^3 spectrum of the ion at m/z 165 from the FDHP **(4)** standard (Figures 4.7F and G, respectively). Together these spectra provide strong evidence that the ion observed at m/z 194 from the reaction of DHNP **(1)** with the Y61F site directed-mutagenesis product of SaDHNA was a mixture of both HPO and FDHP **(4)**, at a ratio of approximately 2:1.

Figure 4.7

A
B
C
D
E
F
G
% Relative Abundance
m/z
[M+H]+
194
-H2O
176
165
[M+H-H2O]+
176
-CO
148
134
108
-NH3
148
[M+H-29]+
165
-H2O
147
136
122
120
100
60
140
180
220

Figure 4.7 (continued) Multistage tandem mass spectrometry identification of m/z 194 product from the reaction of DHNP **(1)** with the Y61F SaDHNA. (A) CID MS/MS product ion spectrum of the ion at m/z 194 obtained from the Figure 4.2B. (B) CID MS/MS product ion spectrum of the m/z 194 precursor ion obtained from a standard solution of HPO. (C) CID MS/MS product ion spectrum of the m/z 194 precursor ion obtained from a standard solution of FDHP **(4)**. (D) CID MS^3 product ion spectrum of the ion at m/z 176 in Figure 4.7A. (E) CID MS^3 product ion spectrum of the ion at m/z 176 in Figure 4.7B. (F) CID MS^3 product ion spectrum of the ion at m/z 165 in Figure 4.7A (G) CID MS^3 product ion spectrum of the ion at m/z 165 in Figure 4.7C.

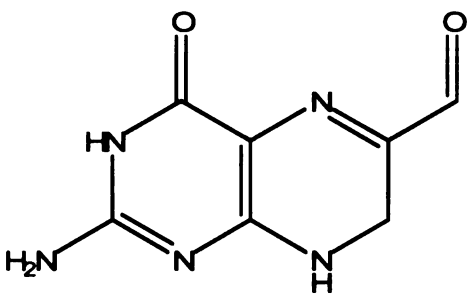

Structure 4: FDHP

The proposed mechanism for the Y61F SaDHNA mutant reaction [65], discussed in more detail later, involves oxygen atom incorporation. In order to determine if the oxygen originated from the solvent, the reaction was run in isotopically labeled $H_2{}^{18}O$. Under these conditions, if the oxygen was from the solvent, the mass spectrum should show a shift in the m/z of the DHXP **(3)** product from 182 to 184. The spectra obtained in the ^{18}O labeled solvent, however, were the same as the spectra obtained when the reaction was run in unlabelled solvent (data not shown), indicating that the oxygen did not originate from the solvent. The oxygen consumption of the reactions was then measured by an oxygraph with an oxygen electrode [65]. The results showed that only the mutant-catalyzed reaction consumed a significant amount of oxygen, indicating that the source of

oxygen for the oxygenation reaction is molecular oxygen dissolved in the buffer, and that Y61F SaDHNA is an oxygenase.

4.4 Mechanisms

4.4.1 Proposed Mechanisms for the Production of HP by the WT SaDHNA

The WT SaDHNA catalyzes both an aldolase and epimerase reaction as shown in Scheme 4.1 [65]. As an aldolase, it converts the natural substrate DHNP **(1)** to HP **(2)** and glycolaldehyde (GA) by a general acid/base reaction involving protonation and deprotonation. The water molecule that is hydrogen bonded to HP **(2)** in the crystal structure (Figure 4.1) is probably the general acid, while the K107 residue, which is hydrogen bonded to the carboxyl group of E22, the hydroxyl group of Y54, and the water molecule, is likely the general base [65]. As an epimerase, DHNA converts DHNP **(1)** to 7,8-dihydromonapterin (DHMP), a stereoisomer of DHNP **(1)**. This reaction is basically the reversal of the step for the formation of the reaction intermediate in forming HP **(2)**, following the flip of GA [65]. For the epimerase reaction, the intermediate species must stay long enough in the active site of the enzyme so that one of the cleaved products can rotate and reattach to form the new stereoisomer. For the aldolase reaction, the two products may be released quickly from the active site of the enzyme. The overall products of these enzymatic reactions may be determined by the relative rates of these processes [54].

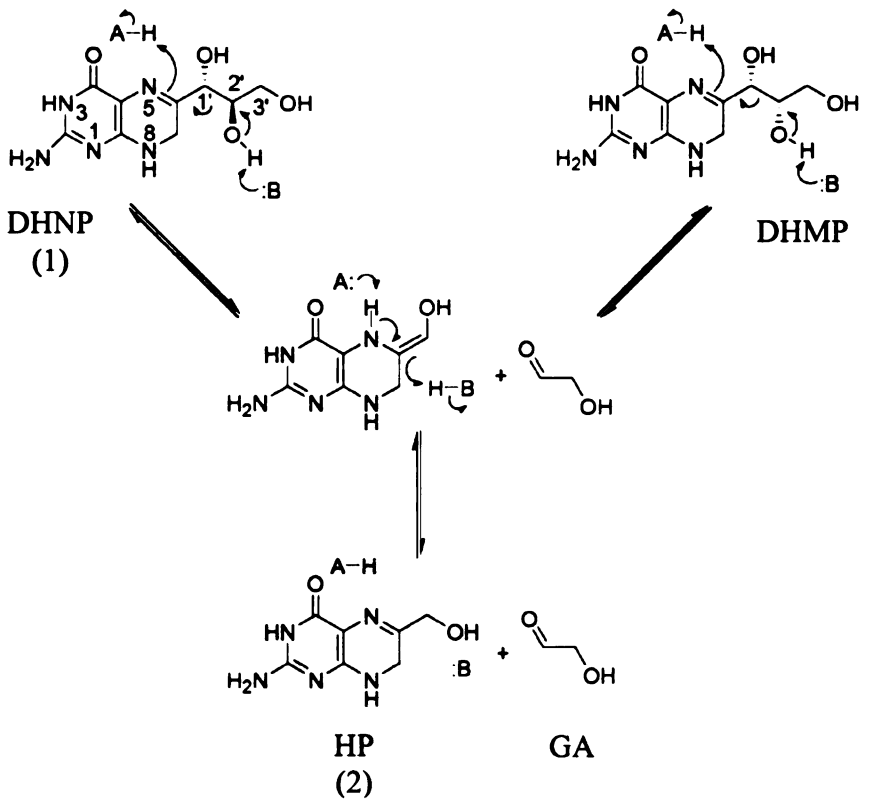

Scheme 4.1 Proposed chemical mechanism for the generation of HP **(2)** by the WT SADHNA. For simplicity, the physical steps of substrate binding and product dissociation are omitted [65].

4.4.2 Proposed Mechanisms for the Production of DHXP by the Y61F SaDHNA

DHXP **(3)** is generated via the same enol intermediate as in the WT enzyme-catalyzed reaction, but this species undergoes an oxygenation reaction to form DHXP **(3)**. The proposed mechanism is shown in Scheme 4.2 and, as with the WT mechanism, the enol intermediate is formed by a protonation/deprotonation step [65]. This enol intermediate is then deprotonated to generate a carbanion species, which donates a single electron to molecular oxygen to form a caged radical pair. The caged radical reacts to generate the peroxide ion, which leads to the formation of DHXP **(3)** and formic acid.

The reaction path for the formation of DHXP **(3)** from the enol intermediate is speculative. However, the presence of formic acid as a reaction product has been confirmed by HPLC [65].

The conserved tyrosine residue plays only a minor role in the physical steps of the enzymatic reaction and the formation of the enol reaction intermediate because the formation of the enol intermediate is not impaired by the mutations to any great extent. It plays a critical role, however, in the protonation of the enol intermediate to form HP **(2)**, since the Y61F catalyzed reaction showed that the major reaction product is DHXP **(3)** rather than HP **(2)** [65]. Molecular oxygen is consumed in the Y61F catalyzed reaction, but not in the WT catalyzed reaction, making the mutant enzyme is an oxygenase, while the WT enzyme is an aldolase. The active site is likely to be accessible to molecular oxygen even in the wild-type enzyme, but the wild-type enzyme is an efficient aldolase rather than an oxygenase because it has a general acid that can efficiently protonate the enol intermediate to form HP **(2)**. Thus, the conserved tyrosine residue plays only a minor role in the formation of the enol reaction intermediate, but a critical role in the protonation of the enol intermediate to form HP **(2)** [65].

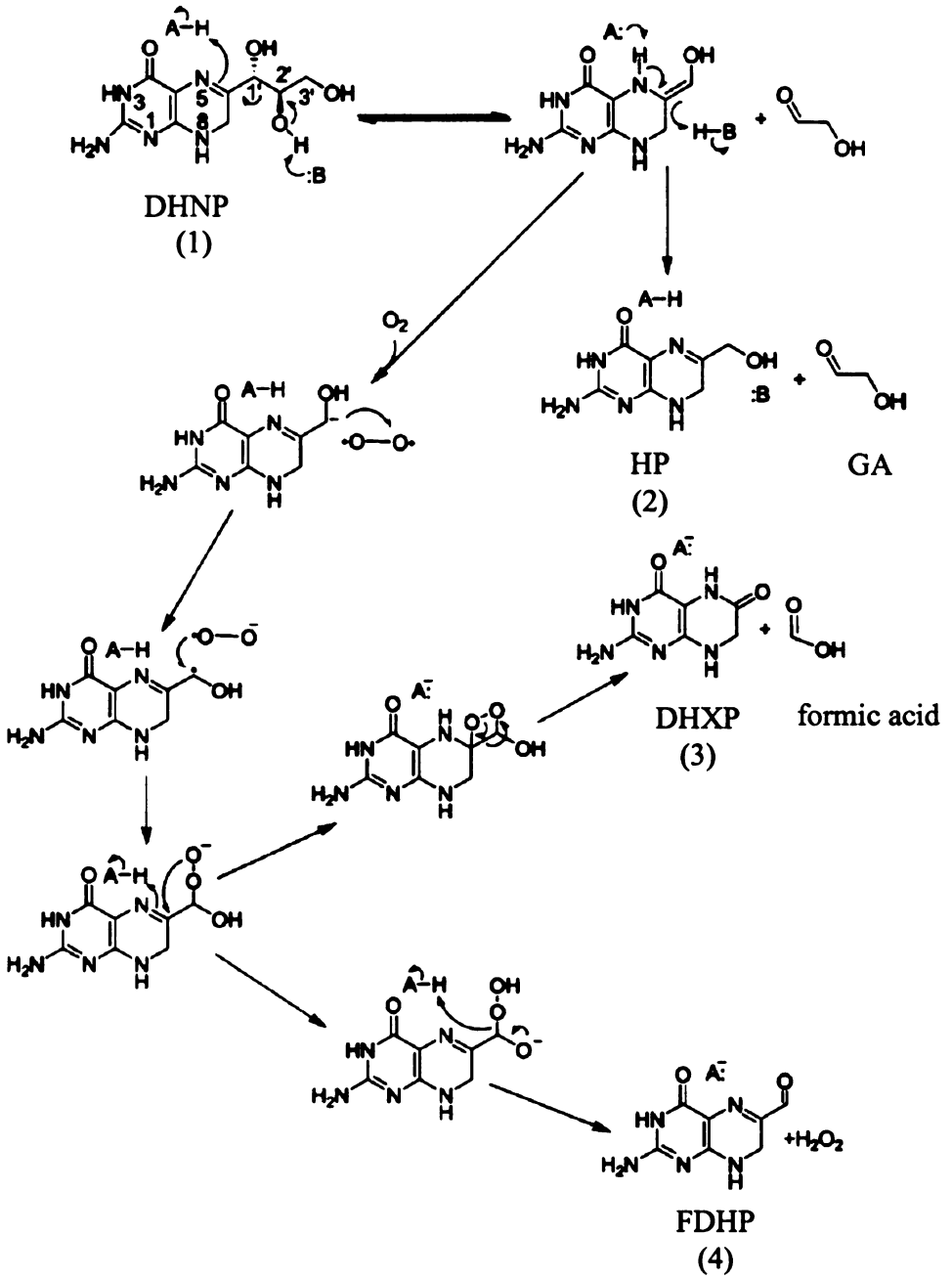

Scheme 4.2 Proposed chemical mechanism for the generation of DHXP **(3)** and FDHP **(4)** by the Y61F SaDHNA. For simplicity, many steps are indicated by single arrows, irrespective of their reversibility [65].

4.5 Conclusions

Like other enzymes in the folate pathway, DHNA is an attractive target for antimicrobial research. The functional role of a conserved tyrosine residue at the active site of DHNA was investigated by site-directed mutagenesis by converting the tyrosine to a phenylalanine (Y61F). The wild-type and mutant substrates reactivity were then characterized by multistage tandem mass spectrometry (MS/MS and MS^3) in a linear ion trap. The wild-type catalyzed reaction gave the expected product HP **(2)**, but the Y61F mutant catalyzed reaction gave the product DHXP **(3)**. By confirming that the product for the WT catalyzed reaction was different than the product for the mutant-catalyzed reaction, it was then proposed that the WT enzyme was an aldolase and the Y61F enzyme was an oxygenase.

REFERENCES

1. Pratt, J. M.; Petty, J.; Riba-Garcia, I.; Robertson, D. H. L.; Gaskell, S. J.; Oliver, S. G.; Beynon, R. J. Dynamics of protein turnover, a missing dimension in proteomics. *Mol. Cell. Proteomics* **2002**, *1*, 579-591.

2. Hanash, S. Disease proteomics. *Nature* **2003**, *422*, 226-232.

3. Karas, M.; Hillenkamp, F. Laser desorption ionization of proteins with molecular masses exceeding 10 000 daltons. *Anal. Chem.* **1988**, *60*, 2299-2301.

4. Fenn, J. B.; Mann, M.; Meng, C. K.; Wong, S. F.; Whitehouse, C. M.; Electrospray ionization for mass spectrometer of large biomolecules. *Science* **1989**, *246*, 64-71.

5. Gomez, A.; Tang, K. Charge and fission of droplets in electrostatic sprays. *Phys. Fluids* **1994**, *6*, 404-414.

6. Thomson, B. T.; Iribarne, J. V. Field induced ion evaporation from liquid surfaces at atmospheric pressure. *J. Chem. Phys.* **1979**, *71*, 4451-4463.

7. Iribarne, J. V.; Thomson, B. T. On the evaporation of small ions from charged droplets. *J. Chem. Phys.* **1976**, *64*, 2287-2294.

8. Charles, M. J.; McLuckey, S. A.; Glish, G. L. Competition between resonance ejection and ion dissociation during resonant excitation in a quadrupole ion trap. *J. Am. Soc. Mass Spectrom.* **1994**, *5*, 1031-1041.

9. Hoffmann, E. D.; Stroobant, V. Mass spectrometry principles and applications, 2nd edition, John Wiley and Sons, New York, 2002.

10. Hager, J. W. A new linear ion trap mass spectrometer. *Rapid Commun. Mass. Spectrom.* **2002**, *16*, 512-526.

11. Schwartz, J. C.; Senko, M. W.; Syka, J. E. A two-dimensional quadrupole ion trap mass spectrometer. *J. Am. Soc. Mass Spectrom.* **2002**, *13*, 659-669.

12. Henzel, W. J.; Billeci, T. M.; Stults, J. T.; Wong, S. C.; Grimley, C.; Watanabe, C. Identifying proteins from two-dimensional gels by molecular mass searching of peptide fragments in protein sequence databases. *Proc. Natl. Acad. Sci. U.S.A.* **1993**, *90*, 5011-5015.

13. Hunt, D. F.; Yates, J. R.; Shabanowitz, J.; Winston, S.; Hauer, C. R. Protein sequencing by tandem mass spectrometry. *Proc. Natl. Acad. Sci. U.S.A.* **1986**, *83*, 6233-6237.

14. Eng, J. K.; McCormack, A. L.; Yates, J. R. An approach to correlate tandem mass spectral data of peptides with amino acid sequences in a protein database. *J. Am. Soc. Mass Spectrom.* **1994**, *5*, 976-989.

15. Perkins, D. N.; Pappin, D. J. C.; Creasy, D. M; Cottrell, J. S. Probability-base protein identification by searching sequence databases using mass spectrometry data. *Electrophoresis* **1999**, *20*, 3551-3567.

16. Chait, B. T.; Kent, S. B. H. Weighing naked proteins: practical, high-accuracy mass measurement of peptides and proteins. *Science* **1992**, *257*, 1885-1894.

17. Scherperel, G.; Yan, H.; Wang, Y.; Reid, G. E. 'Top-down' characterization of site-directed mutagenesis products of Staphylococcus aureus dihydroneopterin aldolase by multistage tandem mass spectrometry in a linear quadrupole ion trap. *The Analyst* **2006**, *131*, 291-302.

18. Marshall. G.; Hendrickson, C. L.; Jackson, G. S. Fourier transform ion cyclotron resonance mass spectrometry: a primer. *Mass Spectrom. Rev.* **1998**, *17*, 1-35.

19. Fridriksson, E. K.; Beavil, A.; Holowka, D.; Gould, H. J.; Baird, B.; McLafferty, F. W. Heterogeneous glycosylation of immunoglobulin E constructs characterized by top-down high-resolution 2-D mass spectrometry. *Biochem.* **2000**, *39*, 3369-3376.

20. Sze, S. K.; Ge, Y.; Oh, H-B.; McLafferty, F. W. Top-down mass spectrometry of a 29-kDa protein for characterization of any posttranslational modification to within one residue. *Proc. Natl. Acad. Sci. U.S.A.* **2002**, *99*, 1774-1779.

21. Meng, F.; Cargille, B. J.; Miller, L. M.; Forbes, A. J.; Johnson, J. R.; Kelleher, N. L. Informatics and multiplexing of intact protein identification in bacteria and the archaea. *Nature. Biotechnol.* **2001**, *19*, 952-957.

22. Meng, F.; Cargille, Y. B. J.; Patrie, S. M.; Johnson, J. R.; McLoughlin, S. M.; Kelleher, N. L. Processing complex mixtures of intact proteins for direct analysis by mass spectrometry. *Anal. Chem.* **2002**, *74*, 2923-2929.

23. Reid, G. E.; Stephenson, J. L.; McLuckey, S. A. Tandem mass spectrometry of ribonuclease A and B: n-Linked glycosylation site analysis of whole protein ions. *Anal. Chem.* **2002**, *74*, 577-583.

24. Kelleher, N. L. Top-down proteomics. *Anal. Chem.* **2004**, *76*, 196A-203A.

25. Kelleher, N. L.; Lin, H. Y.; Valaskovic, G. A.; Aaserud, D. J.; Fridriksson, E. K.; McLafferty, F. W. Top down versus bottom up protein characterization by tandem high-resolution mass spectrometry. *J. Am. Chem. Soc.* **1999**, *121*, 806-812.

26. Reid, G. E.; McLuckey, S. A. 'Top down' protein characterization via tandem mass spectrometry. *J. Mass Spectrom.* **2002**, *37*, 663-675.

27. Hogan, J. M.; Pitteri, S. J.; McLuckey, S. A. Phosphorylation site identification via ion trap tandem mass spectrometry of whole protein and peptide ions: Bovine α-crystallin A chain. *Anal. Chem.* **2003**, *75*, 6509-6516.

28. Shi, S. D.-H.; Drader, J. J.; Hendrickson, C. L.; Marshall, A. G. Fourier transform ion cyclotron resonance mass spectrometry in a high homogeneity 25 Tesla resistive magnet. *J. Am. Soc. Mass Spectrom.* **1999**, *10*, 265–268.

29. Makarov, A. Electrostatic axially harmonic orbital trapping: A high-performance technique of mass analysis. *Anal. Chem.* **2000**, 72, 1156-1162.

30. Hu, Q.; Noll, R. J.; Li, H.; Makarov, A.; Hardman, M.; Cooks, R. G. The Orbitrap: a new mass spectrometer. *J. Mass Spectrom.* **2005**, *40*, 430-443.

31. Xia, Y.; Chrisman, P. A.; Erickson, D. E.; Liu, J.; Liang, X.; Londry, F. A.; Yang, M. J.; McLuckey, S. A. Implementation of ion/ion reactions in a quadrupole/time-of-flight tandem mass spectrometer. *Anal. Chem.* **2006**, 78, 4146-4154.

32. Medzihradszky, K. F.; Zhang, X.; Chalkley, R. J.; Guan, S.; McFarland, M. A.; Chalmers ,M. J.; Marshall, A. G.; Diaz, R. L.; Allis, C. D.; Burlingame, A. L. Characterization of tetrahymena histone H2B variants and posttranslational populations by electron capture dissociation (ECD) fourier transform ion cyclotron mass spectrometry (FT -ICR MS). *Mol. Cell. Proteomics* **2004**, 3, 872-886.

33. Macek, B.; Waanders, L. F.; Olsen, J. V.; Mann, M. Top-down protein sequencing and MS^3 on a hybrid linear quadrupole ion trap-orbitrap mass spectrometer. *Mol. Cell. Proteomics* **2006**, 5, 949-958.

34. Frey, B. L.; Lin, Y.; Westphall, M. S.; Smith, L. M. Controlling gas-phase reactions for efficient charge reduction electrospray mass spectrometry of intact proteins. *J. Am. Soc. Mass Spectrom.* **2005**, *16*, 1876-1887.

35. Stephenson, J. L.; McLuckey, S. A. Simplification of product ion spectra derived from multiply charged parent ions via ion/ion chemistry. *Anal. Chem.* **1998**, *70*, 3533-3544.

36. Reid, G. E.; Wells, J. M.; Badman, E. R.; McLuckey, S. A. Performance of a quadrupole ion trap mass spectrometer adapted for ion/ion reaction studies. *Int. J. Mass Spectrom.* **2003**, *222*, 243-258.

37. Reid, G. E.; Shang, H.; Hogan, J. M.; Lee, G. U.; McLuckey, S. A. Gas-phase concentration, purification, and identification of whole proteins from complex mixtures. *J. Am. Chem. Soc.* **2002**, *124*, 7353-7362.

38. Yan, F.; He, M.; Hogan, J. M.; Rossie, S. S.; McLuckey, S. A. Targeted biomarker detection via whole protein ion trap tandem mass spectrometry: thymosin b4 in a human lung cancer cell line. *J. Mass Spectrom.* **2005**, *40*, 441-451.

39. Amunugama, R.; Hogan, J. M.; Newton, K. A.; McLuckey, S. A. Whole protein dissociation in a quadrupole ion trap: identification of an a priori unknown modified protein. *Anal. Chem.* **2004**, *76*, 720-727.

40. McLuckey, S. A.; Reid, G. E.; Wells, J. M. Ion parking during ion/ion reactions in electrodynamic ion traps. *Anal. Chem.* **2002**, *74*, 336-346.

41. Xia, Y;, Chrisman, P. A.; Erickson, D. E.; Liu, J.; Liang, X.; Londry, F. A.; Yang, M. J.; McLuckey, S. A. Implementation of Ion/Ion Reactions in a Quadrupole/Time-of-Flight Tandem Mass Spectrometer. *Anal. Chem.* **2006**, 78, 4146-4154.

42. Chrisman, P. A.; Pitteri, S. J.; McLuckey, S. A. Parallel ion parking of protein mixtures. *Anal. Chem.* **2006**, *78*, 310-316.

43. Reid, G. E.; Wu, J.; Chrisman, P. A.; Wells, J. M.; McLuckey, S. A. Charge-state-dependent sequence analysis of protonated ubiquitin ions via ion trap tandem mass spectrometry. *Anal. Chem.* **2001**, *73*, 3274-3281.

44. He, M.; Reid, G. E.; Shang, H.; Lee, G. U.; McLuckey, S. A. Dissociation of multiple protein ion charge states following a single gas-phase purification and concentration procedure. *Anal. Chem.* **2002**, *74*, 4653-4661.

45. Schey, K. L.; Cook, L. A.; Hildebrandt, J. D. Ion trap tandem mass spectrometry of intact GTP-binding protein γ-subunits. *Int. J. Mass Spectrom.* **2001**, *212*, 377-388.

46. Claverol, S.; Burlet-Schiltz, O.; Gairin, J. E.; Monsarrat, B. Characterization of protein variants and post-translational modifications: ESI-MS^n analyses of intact proteins eluted from polyacrylamide gels. *Mol. Cell. Proteomics* **2003**, *2*, 483-493.

47. Pesavento, J. J.; Mizzen, C. A.; Kelleher, N. L. Quantitative analysis of modified proteins and their positional isomers by tandem mass spectrometry: human histone H4. *Anal. Chem.* **2006**, *78*, 4271-4280.

48. Cooper, H. J.; Hakansson, K.; Marshall, A. G. The role of electron capture dissociation in biomolecular analysis. *Mass Spectrom. Rev.* **2005**, *24*, 201-222.

49. Syka, J. E. P.; Coon, J. J.; Schroeder, M. J.; Shabanowitz, J.; Hunt, D. F. Peptide and protein sequence analysis by electron transfer dissociation mass spectrometry. *Proc. Natl. Acad. Sci. U.S.A.* **2004**, *101*, 9528-9533.

50. Chrisman, P. A.; Pitteri, S. J.; McLuckey, S. A. Parallel ion parking: improving conversion of parents to first-generation products in electron transfer dissociation. *Anal. Chem.* **2005**, *77*, 3411-3414.

51. Horn, D. M.; Zubarev, R. A.; McLafferty, F. W. Automated reduction and interpretation of high resolution electrospray mass spectra of large molecules. *J. Am. Soc. Mass Spectrom.* **2000**, *11*, 320-332.

52. Taylor, G. K.; Kim, Y-B.; Forbes, A. J.; Meng, F.; McCarthy, R.; Kelleher, N. L. Web and database software for identification of intact proteins using "top down" mass spectrometry. *Anal. Chem.* **2003**, *75*, 4081-4086.

53. Demirev P. A.; Lin, J. S.; Pineda, F.J.; Fenselau, C. Bioinformatics and mass spectrometry for microorganism identification: proteome-wide post-translational modifications and database search algorithms for characterization of intact H. pylori *Anal. Chem.* **2001**, *73*, 4566-4573.

54. Wang, Y. Structure and function relationship of dihydroneopterin aldolases from escherichia coli and staphylococcus aureus, Ph.D. Dissertation, Department of Biochemistry and Molecular Biology, Michigan State University, 2006.

55. Kapp, E. A.; Schuetz, F.; Reid, G. E.; Eddes, J. S.; Moritz, R. L.; O'Hair, R. A. J.; Speed, T. P.; Simpson, R. J. Mining a tandem mass spectrometry database to determine the trends and global factors influencing peptide fragmentation. *Anal. Chem.* **2003**, *75*, 6251-6264.

56. Newton, K. A.; Chrisman, P. A.; Reid, G. E.; Wells, J. M; McLuckey, S. A. Gaseous apomyoglobin ion dissociation in a quadrupole ion trap: $[M + 2H]^{2+} - [M + 21H]^{21+}$. *Int. J. Mass Spectrom.* **2001**, *212*, 359-376.

57. Engel, B. J.; Pan, P.; Reid, G. E.; Wells, J. M.; McLuckey, S. A. Charge state dependent fragmentation of gaseous protein ions in a quadrupole ion trap: bovine ferri-, ferro-, and apo-cytochrome c. *Int. J. Mass Spectrom.* **2002**, *219*, 171-187.

58. Hogan, J. M.; McLuckey, S. A. Charge state dependent collision-induced dissociation of native and reduced porcine elastase. *J. Mass Spectrom.* **2003**, *38*, 245-256.

59. Wysocki, V. H.; Tsaprailis, G.; Smith, L. L.; Breci, L. A. Mobile and localized protons: a framework for understanding peptide dissociation. *J. Mass Spectrom.* **2000**, 35, 1399-1406.

60. Roboz, J. Introduction to mass spectrometry: instrumentation and techniques, John Wiley and Sons, New York, **1968**, 149-179.

61. Prakash, H.; Mazumdar, S. Direct correlation of the crystal structure of proteins with the maximum positive and negative charge states of gaseous protein ions produced by electrospray ionization. *J. Am. Soc. Mass Spectrom.* **2005**, *16*, 1409-1421.

62. Sanders, W. J.; Nienaber, V. L.; Lerner, C. G.; McCall, J. O.; Merrick, S. M.; Swanson, S. J.; Harlan, J. E.; Stoll, V. S.; Stamper, G. F.; Betz, S. F.; Condroski, K. R.; Meadows, R. P.; Severin, J. M.; Walter, K. A.; Magdalinos, P.; Jakob, C. G.; Wagner, R.; Beutel, B. A. Discovery of potent inhibitors of dihydroneopterin aldolase using crystaLEAD high-throughput x-ray crystallographic screening and structure-directed lead optimization. *J. Med. Chem.* **2004**, *47*, 1709-1718.

63. Walsh, C. Where will new antibiotics come from?. *Nat. Rev. Microbiol.* **2003**, *1*, 65-70.

64. Hennig, M.; D'Arcy, A.; Hampele, I. C.; Page, M. G. P.; Oefner, C.; Dale, G. E. Crystal structure and reaction mechanism of 7,8-dihydroneopeterin aldolase from *Staphylococcus aureus*. *Nat. Struct. Biol.* **1998**, *5*, 357-362.

65. Wang, Y.; Scherperel, G.; Roberts, K. D.; Jones, A. D.; Reid, G. E.; Yan, H. A point mutation coverts dihydroneopterin aldolase to a cofactor-independent oxygenase. *J. Am. Chem. Soc.* **2006**, *128*, 13216-13223.